A Virtual Element Method for the Two-Phase Flow of Immiscible Fluids in Porous Media

A Virtual Element Method for the Two-Phase Flow of Immiscible Fluids in Porous Media

S. Berrone*,†, M. Busetto*

Abstract

A primal C^0-conforming virtual element discretization for the approximation of the bidimensional two-phase flow of immiscible fluids in porous media using general polygonal meshes is discussed. This work represents a first investigation of the potentialities of the Virtual Element Method (VEM) in solving this specific complex problem involving a time-dependent coupled system of nonlinear partial differential equations. The performance of the fully discrete scheme is thoroughly analysed testing it on general meshes considering both a regular problem and more realistic benchmark problems that are of interest for physical and engineering applications.

Keywords: virtual element method, two-phase immiscible flow, porous media, polygonal meshes.

1 Introduction

The Virtual Element Method (VEM) is a very recent extension of the Finite Element Method (FEM) that allows to solve partial differential equations using general polygonal (polyhedral) tessellations of the domain rather than more standard triangular (tetrahedral) or quadrilateral (hexahedral) grids. The main idea of the VEM is to use an approximation of the problem constructed on polytopal elements through the definition of suitable projections onto the space of polynomials that can be computed only on the basis of the degrees of freedom. The use of general polygonal (polyhedral) meshes brings forth several advantages including better domain meshing and approximation of geometric features, use of non-conforming grids and easier mesh adaptivity [1]. All these features are very attractive especially in tackling problems characterized by complex geometries.

The VEM was firstly formulated in [2] as a C^0-conformal method for the solution of the two-dimensional Poisson problem. A non-conformal version was presented in [3]. Then, making use of the enhancement techniques presented in [4], the original C^0-conforming VEM was extended to reaction-diffusion problems with constant coefficients in two and three dimensions and to convection-reaction-diffusion problems characterized by variable coefficients [5]. Its non-conformal counterpart was presented in [6] and [7]. Moreover, VEM has been applied to the solution of time-dependent problems such as parabolic problems [8] and hyperbolic problems [9]. A possible extension of the Virtual Element framework to the discretization of $H(div)$-conforming vector fields was proposed in [10] and further analysed in [11] for the solution of general linear second order elliptic problems in mixed form allowing for variable coefficients. Finally, in [12] the Serendipity VEM spaces were introduced allowing a reduction of the degrees of freedom with respect to the traditional VEM space. A framework for the numerical implementation of the method was firstly presented in [13].

Since the potentialities of the VEM the numerical mathematics and engineering communities have developed a growing interest also in the application of this method to a vast variety of physical and engineering problems. Consequently, the VEM has been used to solve problems in fields such

*Department of Mathematical Sciences "Giuseppe Luigi Lagrange", Politecnico di Torino, 10129 Torino, Italy (stefano.berrone@polito.it, martina.busetto@polito.it), member of INdAM GNCS.

†Member of SmartData@PoliTO.

us fluid dynamics ([14], [15]), solid mechanics ([16], [17], [18]), discrete fracture network simulations ([19], [20], [21], [22]) and electromagnetism [23]. Even if the VEM framework has been extended to a such a vast number of different applications, the literature on VEM for non-linear problems is still relatively youth. Paper [24] can be regarded as the first attempt at using the newborn VEM to solve a non-linear problem. Other examples of applications to semilinear problems can be found in [25] or [26] and to quasilinear problem in [27] or [28]. Despite this, there exist still very few applications to complex and realistic geological flow models related to porous media. The very recent work presented in [29] can be considered as the first investigation on this topic.

In the present work we develop a primal virtual element formulation for the approximation of the two-phase flow equations of immiscible fluids in porous media and we investigate the performance of the fully discrete scheme numerically. We underline that the problem considered here is different from the one of miscible fluids investigated in [29]. Indeed, in our problem, the underlying physical assumption of immiscibility of the fluids involves a different set of equations to be solved. These equations share some of the difficulties discussed in [29], but they also pose their distinctive peculiar problems.

The two-phase flow equations for immiscible fluids are important in many scientific and industrial areas including petroleum and chemical engineering ([30], [31]), hydrogeology [32] and nuclear waste disposal safety [33]. The standard mathematical model for these types of problems consists of a continuity equation and an extended Darcy's law for each one of the two phases plus additional constitutive relationships for the capillary pressure and the relative permeabilities. This approach gives rise to a problem characterized by coupling as well as strong non-linearity of the involved equations. Indeed, the two-phase immiscible fluid flow model in porous media is a coupled system of non-linear time-dependent partial differential equations [30]. This poses severe difficulties in the numerical treatment. As a consequence, different numerical techniques have been developed and we underline that nowadays there exists a large literature with many competitive schemes ([30], [32], [34]). To cope with the coupled nature of the problem, among the various strategies there are the fully implicit methods (FIM) and the operator splitting techniques (IMPES, IMPIS). The former involve the implicit discretization of each equation of the coupled system and the simultaneous solution for all the involved primary unknowns. Whereas, the latter two involve an operator splitting to decouple the equations. For what concerns the space discretization these schemes usually adopt finite elements, finite volumes and discontinuous Galerkin methods.

The purpose of this work is to show that a resolution of the two-phase flow equations for immiscible fluids by means of the VEM allows to exploit all the benefits and the potentialities of this method such as flexibility in terms of meshes, possibility to deal with complicated geometries quite common in geophysical applications and simplified construction of high-order and high-regularity approximations.

In this paper we propose a variant of the IMPIS based approach coupled with the VEM for the space discretization. More precisely, in our approach we introduce an iterative IMPIS method for the solution of the fully implicit system resulting from the time discretization of the two-phase flow equations. In this way, at each iteration, we split the whole system of equations into a saturation and a pressure equation. Then, we discretize the resulting equations in space through the use of the VEM. The virtual element discretization presented here is based on the C^0-conforming virtual element spaces introduced in [4] that through an enhancement technique allows the computation of the local L^2-projection of virtual element functions onto polynomials. Moreover, we also refer to the VEM proposed in [5], [7] and [28] for the discretization of problems with non-constant coefficients and the evaluation of non-linear coefficients through their elementwise polynomial projection.

After proposing the method, we test the numerical scheme in two different ways evaluating it in terms of stability, convergence as well as accuracy. Firstly, we consider a problem with known analytical solution similar to the one proposed in [35], in order to validate the convergence properties. Then, we consider two more realistic benchmark problems taken from [36] and [37] in order to compare our numerical solution with the ones presented in literature. The first test is the McWhorter and Sunada bidirectional flow problem and it involves a parabolic equation for the saturation dominated by a strong diffusive nature. The second test is the McWhorter and Sunada unidirectional flow and it consists of a parabolic equation for the saturation eventually degenerating into a hyperbolic equation due to the possibly small contribute of the diffusive term.

Approaching the degenerate case the saturation solution starts to exhibit oscillations. Therefore, we have adopted a non-linear stabilization technique known as nodal Gradient Jump Viscosity method (nGJV) [38] that has provided good results in smoothing or even eliminating the oscillatory behaviors in case of a sufficiently refined mesh.

Throughout the paper, we will adopt the following notation for the Sobolev spaces and norms. Given an open and bounded domain D, $s \in \mathbb{N} \cup \{\infty\}$, and $p \in \mathbb{N}$, we define by $W^{s,p}(D)$ the space of all L^p integrable functions over D whose weak derivatives up to order s are in the space of all L^p integrable functions. We will use $|\cdot|_{s,D}$ and $||\cdot||_{s,D}$ to denote the seminorm and norm, respectively, in the Sobolev space $H^s(D) := W^{s,2}$, and $(\cdot,\cdot)_D$ will denote the $L^2(D)$ inner product. The subscript D is omitted when D coincides with the computational domain. Moreover, $|\cdot|$ is the standard Euclidean norm for either scalars or vectors. Finally, $\mathbb{P}_l(D)$ is the space of polynomials of degree less or equal to l on the domain D and $[\mathbb{P}_l(D)]^2$ the corresponding polynomial vector values space. Conventionally, $\mathbb{P}_{-1}(D) = \{0\}$.

The structure of this work is as follows. In Section 2, we state the model problem and its governing equations. In Section 3, we introduce the time discretization and the adopted iterative approach. In Section 4, we describe the proposed spatial virtual element discretization. In Section 5, we summarize the complete numerical resolution algorithm. In Section 6, we focus on the convergence results solving the equations for cases in which the analytical solution is known. In Sections 7 and 8, we present and discuss the numerical resolution of some benchmark problems. Finally, in Section 9 we draw some conclusions.

2 Governing differential equations

A porous medium is a material composed of a solid part known as porous matrix and a void space that can be filled with fluids. In particular, in a two-phase immiscible flow the void space is filled with two immiscible fluids. From a physical point of view the two fluids are typically distinguished into wetting phase (w) and non-wetting phase (n) according to the interaction between the adhesive and cohesive forces that results into a different contact angle with the solid surface.

Let us consider a space-time domain $Q_T := \Omega \times \mathcal{I}_T$, where Ω is an open bounded measurable subset of $\mathbb{R}^2$ with Lipschitz boundary $\Gamma := \partial\Omega$ of unit normal $\boldsymbol{n}$ pointing outward and $\mathcal{I}_T := [0, T]$ with $T \in \mathbb{R}^+$, is a time interval. Physically, the space domain Ω represents the porous medium. Then, the general mathematical problem of the two-phase flow of immiscible fluids in a porous medium reads:

Find $S_\alpha(\boldsymbol{x}, t)$, $\boldsymbol{u}_\alpha(\boldsymbol{x}, t)$ and $p_\alpha(\boldsymbol{x}, t)$, with $\alpha = n, w$ and $(\boldsymbol{x}, t)$ in the space-time domain Q_T such that

$$\begin{cases} \frac{\partial(\Phi\rho_\alpha S_\alpha)}{\partial t} + \nabla \cdot (\rho_\alpha \boldsymbol{u}_\alpha) = \rho_\alpha q_\alpha \\ \boldsymbol{u}_\alpha = -\frac{k_{r_\alpha}}{\mu_\alpha} \boldsymbol{K}(\nabla p_\alpha - \rho_\alpha \boldsymbol{g}) \\ S_w + S_n = 1 \\ p_n - p_w = p_c \\ + \text{ boundary and initial conditions.} \end{cases} \tag{1}$$

The unknown physical quantities are: the saturation for each phase $S_\alpha = S_\alpha(\boldsymbol{x}, t) \in [0, 1]$ $[-]$, the Darcy velocity for each phase $\boldsymbol{u}_\alpha = \boldsymbol{u}_\alpha(\boldsymbol{x}, t)$ $[m{\cdot}s^{-1}]$ (volume of fluid flowing per unit time through a unit cross-sectional area normal to the direction of flow), and the single phase pressures $p_\alpha = p_\alpha(\boldsymbol{x}, t)$ $[Pa]$.

The physical data appearing in the equations are: the porosity of the medium $\Phi = \Phi(\boldsymbol{x}, t) \in L^\infty(Q_T)$ $[-]$, the absolute permeability of the medium $\boldsymbol{K} = \boldsymbol{K}(\boldsymbol{x}) \in [L^\infty(\Omega)]^{2\times 2}[m^2]$ that is a symmetric and positive definite tensor, the density for each phase $\rho_\alpha = \rho_\alpha(\boldsymbol{x}, t) \in L^\infty(Q_T)$ $[Kg{\cdot}m^{-3}]$, the scalar source/sink terms $q_\alpha = q_\alpha(\boldsymbol{x}, t) \in L^2(Q_T)$ $[s^{-1}]$, the relative permeability for each phase $k_{r_\alpha} = k_{r_\alpha}(S_\alpha) \in L^\infty([0, 1])$ $[-]$, the dynamic viscosity for each phase $\mu_\alpha = \mu_\alpha(\boldsymbol{x}, t) \in L^\infty(Q_T)$ $[Pa \cdot s]$, the gravity acceleration vector $\boldsymbol{g} \in \mathbb{R}^2$ $[m \cdot s^{-2}]$, the capillary pressure $p_c = p_c(S_\alpha) \in W^{1,\infty}([0, 1])$ $[Pa]$ [39].

We assume that there exist constants ϕ_0, ϕ_1, K_0, $\rho_{\alpha,0}$, $\mu_{\alpha,0} \in \mathbb{R}^+$ such that $\phi_0 < \phi_1 < 1$ and $\phi_0 \le \Phi \le \phi_1$, $\rho_{\alpha,0} \le \rho_\alpha$, $\mu_{\alpha,0} \le \mu_\alpha$, a.e. in Q_T, and $||\boldsymbol{K}||_{L^\infty(\Omega)} \ge K_0$, a.e. in Ω.

The relative permeabilities k_{r_α} and the capillary pressure p_c are considered to be functions of the saturations S_α. We model these relations adopting the Brooks-Corey empirical model [40] that is typically used to describe a physical system with water as wetting phase and a liquid such as oil as non-wetting phase. Firstly, we define the effective saturations $\bar{S}_w$ and $\bar{S}_n$ as

$$\bar{S}_w := \frac{S_w - S_{wr}}{1 - S_{wr} - S_{nr}}, \quad \bar{S}_n := \frac{S_n - S_{nr}}{1 - S_{wr} - S_{nr}},$$

where S_{wr} and S_{nr} are the residual saturations of the wetting and of the non-wetting phase, respectively. It can be easily verified that $\bar{S}_w, \bar{S}_n \in [0,1]$ and $\bar{S}_n + \bar{S}_w = 1$ in Q_T. Then, the capillary pressure-saturation function p_c is modelled as

$$p_c(S_w) = p_d \bar{S}_w^{-\frac{1}{\mu}},$$

where p_d is the entry pressure of the porous medium. Whereas, the relative permeabilities k_{rw} and k_{rn} are modelled in the following way

$$k_{rw}(S_w) = \bar{S}_w^{\frac{2+3\mu}{\mu}}, \quad k_{rn}(S_n) = \bar{S}_n^2\Big(1 - (1 - \bar{S}_n)^{\frac{2+\mu}{\mu}}\Big).$$

From system of equations (1) it can be seen that the two-phase flow model for immiscible fluids in porous media is described by a coupled system of non-linear time-dependent partial differential equations. This system can be rewritten adopting different formulations. In what follows we exploit the so-called pressure-saturation formulation [41]. In this approach the saturation of the wetting-phase S_w and the pressure of the non-wetting phase p_n are selected as the two primary variables. Moreover, we assume incompressibility of the fluids, i.e., the densities of the two phases are constant both in space and in time, and time-independence of the porosity of the medium, i.e., the solid matrix is not poroelastic.

Under these assumptions, system of equations (1) can be rewritten as follows

$$\begin{cases} \nabla \cdot \boldsymbol{u} = q, & \text{(2a)} \\ \Phi \dfrac{\partial S_w}{\partial t} + \nabla \cdot \boldsymbol{u}_w = q_w, & \text{(2b)} \end{cases}$$

where $\boldsymbol{u} := \boldsymbol{u}_w + \boldsymbol{u}_n$ $[m \cdot s^{-1}]$ is the total velocity and $q := q_w + q_n$ $[s^{-1}]$ is the scalar total source/sink term. Moreover, we rewrite $\boldsymbol{u}$ and $\boldsymbol{u}_w$ as functions of p_n and S_w

$$\begin{aligned} \boldsymbol{u} &= -\boldsymbol{K}\lambda \nabla p_n + \boldsymbol{K}\lambda_w \nabla p_c + \boldsymbol{K}(\lambda_w \rho_w + \lambda_n \rho_n)\boldsymbol{g}, & \text{(3)} \\ \boldsymbol{u}_w &= f_w \boldsymbol{u} + \boldsymbol{K} f_w \lambda_n \nabla p_c + \boldsymbol{K} f_w \lambda_n (\rho_w - \rho_n)\boldsymbol{g} \\ &= \boldsymbol{K}\lambda_w \nabla p_c - \boldsymbol{K}\lambda_w \nabla p_n + \boldsymbol{K}\lambda_w \rho_w \boldsymbol{g}. & \text{(4)} \end{aligned}$$

The new quantities appearing in Equations (3)-(4) are the phase mobility for each phase $\lambda_\alpha(\boldsymbol{x}, t; S_\alpha) := k_{r\alpha}(S_\alpha)/\mu_\alpha(\boldsymbol{x}, t) \in L^\infty(Q_T \times [0,1])$ $[Pa \cdot s]^{-1}$, the total mobility $\lambda(\boldsymbol{x}, t; S_w) := \lambda_n + \lambda_w \in L^\infty(Q_T \times [0,1])$ $[Pa \cdot s]^{-1}$ and the fractional flow for the wetting phase $f_w := \lambda_w/\lambda \in L^\infty(Q_T \times [0,1])$ $[-]$. We note that thanks to the previous assumptions $\lambda_\alpha \geq 0$, a.e. in $Q_T \times [0,1]$. Moreover, since both the relative permeabilities are positive and non-zero at the same saturation value, there exists a constant $\lambda_0 \in \mathbb{R}^+$ such that $\lambda_0 \leq \lambda$, a.e. in $Q_T \times [0,1]$. Finally, the pressure-saturation formulation reads:

Find $S_w(\boldsymbol{x}, t)$ and $p_n(\boldsymbol{x}, t)$ such that the following holds true in Q_T

$$\begin{cases} -\nabla \cdot \Big\{ \boldsymbol{K}\lambda \nabla p_n - \boldsymbol{K}\lambda_w \dfrac{dp_c}{dS_w} \nabla S_w - \boldsymbol{K}(\lambda_w \rho_w + \lambda_n \rho_n)\boldsymbol{g} \Big\} = q, & \text{(5a)} \\ \Phi \dfrac{\partial S_w}{\partial t} + \nabla \cdot \Big\{ \boldsymbol{K}\lambda_w \dfrac{dp_c}{dS_w} \nabla S_w - \boldsymbol{K}\lambda_w \nabla p_n + \boldsymbol{K}\lambda_w \rho_w \boldsymbol{g} \Big\} = q_w. & \text{(5b)} \end{cases}$$

The derivative of the capillary pressure $\frac{dp_c}{dS_w}$ is negative. Therefore, the term $\nabla \cdot \Big(\boldsymbol{K}\lambda_w \frac{dp_c}{dS_w} \nabla S_w\Big)$ can be thought as $-\nabla \cdot \Big(\boldsymbol{K}\lambda_w \Big|\frac{dp_c}{dS_w}\Big| \nabla S_w\Big)$, i.e., it is a stabilizing diffusive term.

Equation (5a) is called the *pressure equation* and it is an elliptic equation with respect to p_n, whereas Equation (5b) is called the *saturation equation* and it is either a non-linear hyperbolic equation with respect to S_w if the capillary pressure p_c is neglected ($p_c = 0$) or a parabolic convection-diffusion equation with respect to S_w if the capillary pressure p_c is not neglected ($p_c \neq 0$) [31]. In this latter case, it can also be convection dominated having a possible degenerate parabolic nature. System of equations (5a)-(5b) is completed by boundary conditions for the pressure of the non-wetting phase p_n and for the saturation of the wetting phase S_w and by initial conditions for the saturation of the wetting phase S_w. We decompose the boundary of the domain as $\partial\Omega := \Gamma_{N_p} \cup \Gamma_{D_p} = \Gamma_{N_S} \cup \Gamma_{D_S}$, with $\Gamma_{N_p} \cap \Gamma_{D_p} = \Gamma_{N_S} \cap \Gamma_{D_S} = \emptyset$, where Γ_{N_p} and Γ_{D_p} refer to the Neumann boundary and Dirichlet boundary, respectively, related to p_n, and Γ_{N_S} and Γ_{D_S} refer to the Neumann boundary and the Dirichlet boundary, respectively, related to S_w. Then, we consider the following Dirichlet and Neumann boundary conditions for both p_n and S_w, and the following initial condition for S_w

$$\begin{cases} p_n = g_{D_p}, & \text{on } \Gamma_{D_p} \times \mathcal{I}_T, \\ \boldsymbol{u} \cdot \boldsymbol{n} = Q_{N_p}, & \text{on } \Gamma_{N_p} \times \mathcal{I}_T, \\ S_w = g_{D_S}, & \text{on } \Gamma_{D_S} \times \mathcal{I}_T, \\ \boldsymbol{u}_w \cdot \boldsymbol{n} = Q_{N_S}, & \text{on } \Gamma_{N_S} \times \mathcal{I}_T, \\ S_w(0) = S_{w0}, & \text{in } \ \Omega \times \{0\}. \end{cases}$$

Equations (5a)-(5b) are non-linearly coupled. In Equation (5a) the coupling is through the mobilities λ, λ_w and λ_n and the capillary pressure p_c that all depend on S_w. Whereas, in Equation (5b) the coupling is through the gradient of p_n. In order to cope with both the coupling and the non-linearity of this system of equations, different techniques have been proposed in literature. The most famous ones are: *IMplicit-Pressure-Explicit-Saturation* methods (IMPES), *IMplicit-Pressure-Implicit-Saturation* methods (IMPIS), and *Fully Implicit Methods* (FIM) ([30], [34], [42], [43]).

In what follows, we adopt an improved version of the IMPIS method, that we refer as *iterative* IMPIS. The idea is to use IMPIS as an iterative scheme for the solution of the fully implicit system arising from the time discretization of (5a)-(5b). At each iteration of this approach we split the whole system of equations into a saturation equation and a pressure equation, we discretize them in space through the use of the Virtual Element Method and finally, we solve them in sequence and implicitly as in the traditional IMPIS approach. For the sake of simplicity, in Sections 3, 4 and 5 we consider homogeneous Dirichlet boundary conditions for both the pressure p_n and the saturation S_w.

3 Time discretization

Given the time interval $\mathcal{I}_T$, we subdivide it into C time steps $\Delta t^n := t^n - t^{n-1}$ $(n = 1, ..., C)$ with $0 = t^0 < t^1 < ... < t^C = T$. Then, we focus on the time discretization of problem (5a)-(5b). More precisely, given a time sub-interval $[t^n, t^{n+1}]$, we proceed as follows. Firstly, we assume that the pressure $p_n(t^n)$ and the saturation $S_w(t^n)$ at the beginning of the sub-interval are known. Then, we use the Crank-Nicolson scheme for the time discretization of Equation (5b) and, since no time derivative appears in Equation (5a), we simply evaluate it at the end of the sub-interval, that is, at t^{n+1}. Finally, the variational formulation reads as follows.

Given $p_n(t^n),\ S_w(t^n) \in H^1_0(\Omega)$*, find* $p_n(t^{n+1}),\ S_w(t^{n+1}) \in H^1_0(\Omega)$*, for* $n = 0, 1, \ldots, C-1$*, such that the following holds true* $\forall v_p,\ v_S \in H^1_0(\Omega)$

$$\begin{cases} a(S_w(t^{n+1}); p_n(t^{n+1}), v_p) = F^P_{t^{n+1}}(S_w(t^{n+1}), v_p), & \text{(6a)} \\ \dfrac{c(S_w(t^{n+1}), v_S) - c(S_w(t^n), v_S)}{\Delta t} = \\ \dfrac{1}{2} F^S_{t^{n+1}}(S_w(t^{n+1}), S_w(t^{n+1}), p_n(t^{n+1}), v_S) + \dfrac{1}{2} F^S_{t^n}(S_w(t^n), S_w(t^n), p_n(t^n), v_S). & \text{(6b)} \end{cases}$$

where

$$F^P_t(z, w) := (q(t), w)_\Omega - b(z, w) - g(z, w),$$

$$F_t^S(z_1, z_2, v, w) := (q_w(t), w)_\Omega - d(z_1; z_2, w) - e(z_1, v, w) - f(z_1, w).$$

The other quantities are defined as follows. $a(\cdot;\cdot,\cdot)$ is the global form bilinear and symmetric in its second and third arguments defined as

$$a(z; v, w) := \int_\Omega \nabla v^T \boldsymbol{K} \lambda(z) \nabla w \ \mathrm{d}\mathbf{x}.$$

Moreover, $b(\cdot,\cdot)$ and $g(\cdot,\cdot)$ are defined as

$$b(z, w) := -\int_\Omega \nabla z^T \boldsymbol{K} \lambda_w(z) \frac{dp_c(z)}{dS_w} \nabla w \ \mathrm{d}\mathbf{x},$$
$$g(z, w) := -\int_\Omega \boldsymbol{g}^T \boldsymbol{K} (\lambda_w(z)\rho_w + \lambda_n(z)\rho_n) \nabla w \ \mathrm{d}\mathbf{x}.$$

$c(\cdot,\cdot)$ is a global symmetric and bilinear form and $d(\cdot;\cdot,\cdot)$ is a global form symmetric and bilinear in its second and third arguments defined as

$$c(v, w) := \int_\Omega \Phi \ v \ w \ \mathrm{d}\mathbf{x},$$
$$d(z_1; z_2, w) := -\int_\Omega \nabla z_2^T \boldsymbol{K} \lambda_w(z_1) \frac{dp_c(z_1)}{dS_w} \nabla w \ \mathrm{d}\mathbf{x}.$$

Moreover, $e(\cdot;\cdot,\cdot)$ and $f(\cdot,\cdot)$ are defined as

$$e(z_1; v, w) := \int_\Omega \nabla v^T \boldsymbol{K} \lambda_w(z_1) \nabla w \ \mathrm{d}\mathbf{x},$$
$$f(z_1, w) := -\int_\Omega \boldsymbol{g}^T \boldsymbol{K} \lambda_w(z_1) \rho_w \nabla w \ \mathrm{d}\mathbf{x}.$$

System of equations (6a)-(6b) is fully implicit and coupled and it cannot be solved directly because of its non-linearity. However, we can solve it through an iterative method. To this aim, we firstly linearize Equation (6b) only with respect to the saturation using Newton-Raphson method. Then, we adopt an iterative IMPIS formulation for solving equations (6a) and the linearized version of (6b). More precisely, we proceed as follows. Given the initial iterates $p_n(t^{n+1}, 0) := p_n(t^n)$ and $S_w(t^{n+1}, 0) := S_w(t^n)$, we construct a sequence $p_n(t^{n+1}, \hat{k}+1)$ and a sequence $S_w(t^{n+1}, \hat{k}+1) := S_w(t^{n+1}, \hat{k}) + \delta S_w(t^{n+1}, \hat{k}+1)$, $\hat{k} \geq 0$, by solving at each iteration sequentially the linearized problems (1) and (2) that follow. The resulting formulation of the problem reads as:

1. *Given* $S_w(t^n)$, $S_w(t^{n+1}, \hat{k}) \in H_0^1(\Omega)$ *and* $p_n(t^n)$, $p_n(t^{n+1}, \hat{k}) \in H_0^1(\Omega)$, *find* $\delta S_w(t^{n+1}, \hat{k}+1) \in H_0^1(\Omega)$, $\hat{k} \geq 0$, *such that the following holds true* $\forall v_S \in H_0^1(\Omega)$

$$\begin{aligned} &c(\delta S_w(t^{n+1}, \hat{k}+1), v_S) + \frac{\Delta t}{2} \tilde{F}^S(S_w(t^{n+1}, \hat{k}), \delta S_w(t^{n+1}, \hat{k}+1), p_n(t^{n+1}, \hat{k}), v_S) = \\ &- c(S_w(t^{n+1}, \hat{k}), v_S) + \frac{\Delta t}{2} F_{t^{n+1}}^S(S_w(t^{n+1}, \hat{k}), S_w(t^{n+1}, \hat{k}), p_n(t^{n+1}, \hat{k}), v_S) \\ &+ c(S_w(t^n), v_S) + \frac{\Delta t}{2} F_{t^n}^S(S_w(t^n), S_w(t^n), p_n(t^n), v_S), \end{aligned} \tag{7}$$

where

$$\tilde{F}^S(z_1, z_2, v, w) := d(z_1; z_2, w) + l(z_1; z_2, w) + m(z_1; v; z_2, w) + n(z_1; z_2, w),$$

$$l(z_1; z_2, w) := -\int_\Omega z_2 \ (\nabla z_1)^T \boldsymbol{K} b(z_1) \ \nabla w \ \mathrm{d}\mathbf{x},$$
$$m(z_1; v; z_2, w) := \int_\Omega z_2 \ (\nabla v)^T \boldsymbol{K} r(z_1) \ \nabla w \ \mathrm{d}\mathbf{x},$$

$$n(z_1; z_2, w) := -\int_\Omega z_2 \; \boldsymbol{g}^T \boldsymbol{K} r(z_1) \rho_w \; \nabla w \; \mathrm{d}\mathbf{x},$$

$$b := \frac{d}{dS_w}\Big(\lambda_w \frac{dp_c}{dS_w}\Big), \quad r := \frac{d\lambda_w}{dS_w}.$$

2. *Given* $S_w(t^{n+1}, \hat{k}+1) = S_w(t^{n+1}, \hat{k}) + \delta S_w(t^{n+1}, \hat{k}+1)$*, find* $p_n(t^{n+1}, \hat{k}+1) \in H_0^1(\Omega)$*,* $\hat{k} \geq 0$*, such that the following holds true* $\forall v_p \in H_0^1(\Omega)$

$$a(S_w(t^{n+1}, \hat{k}+1); p_n(t^{n+1}, \hat{k}+1), v_p) = F^P_{t^{n+1}}(S_w(t^{n+1}, \hat{k}+1), v_p). \tag{8}$$

Since $S_w(t^{n+1}, \hat{k}+1)$ is known, Equation (8) turns out to be a linear elliptic problem for the pressure $p_n(t^{n+1}, \hat{k}+1)$. Moreover, we notice that even if no time derivative appears in (8), this is still a time dependent problem since saturation and all the parameters that depend on it change at each time. The parameter λ in the bilinear form $a(\cdot;\cdot,\cdot)$ depends on $S_w(t^{n+1}, \hat{k}+1)$, but, as explained in Section 2, λ is bounded from above and from below. Lax-Milgram theorem provides uniqueness for the pressure in $H_0^1(\Omega)$ if the linear functional $F^p_{t^{n+1}}(S_w(t^{n+1}, \hat{k}+1), v_p)$ is bounded for all $v_p \in H_0^1(\Omega)$ and any given $S_w(t^{n+1}, \hat{k}+1)$. In the case of the Brooks-Corey constitutive relations the pressure formulation requires no restriction on the range of $S_w(t^{n+1}, \hat{k}+1)$. Indeed, when the saturation approaches zero, even if $\frac{dp_c}{dS_w}$ is unbounded, the product $\lambda_w \frac{dp_c}{dS_w}$ is bounded. Since $S_w(t^{n+1}, \hat{k})$ and $p_n(t^{n+1}, \hat{k})$ are known, Equation (7) is the time-discrete and linearized version of a parabolic or a possibly degenerate parabolic problem (according to the value of the capillary pressure p_c). Therefore, at each iteration it can be seen as a diffusion-convection-reaction equation for the saturation $S_w(t^{n+1}, \hat{k}+1)$.

4 Space discretization

Let $\mathcal{T}_\delta$ be a tessellation of $\Omega \subset \mathbb{R}^2$ into non-overlapping and not self-intersecting polygons such that the diameter δ_E of each element $E \in \mathcal{T}_\delta$ is bounded by δ. Each polygon E can have a different number of edges with respect to the others and we denote by $\mathcal{E}_{\delta,E}$ the set of its edges. To be more precise, we assume that each element E of the tessellation is star-shaped with respect to every point of a disk of radius $\rho^E \delta_E$, where ρ^E is such that there exists $\rho_0 > 0$ independent of δ so that $\rho_E \geq \rho_0$. Moreover, we assume that every edge of E has length $|e| \geq \rho^E \delta_E$. However, as explained in [5], these assumptions can be relaxed.

We introduce the following elementwise projection operators on the tessellation $\mathcal{T}_\delta$.

- $H^1(E)$*-orthogonal projection operator* $\Pi^\nabla_{k,E} : H^1(E) \to \mathbb{P}_k(E)$ with $k \in \mathbb{N}$, defined as

$$(\nabla \Pi^\nabla_{k,E}(v), \nabla p)_E = (\nabla v, \nabla p)_E, \;\; \forall p \in \mathbb{P}_k(E), \;\; v \in H^1(E),$$

  with the additional conditions to take care of the constant part and uniquely determine $\Pi^\nabla_{k,E}$

$$\begin{aligned} (\Pi^\nabla_{k,E}(v), 1)_{\partial E} &= (v, 1)_{\partial E}, && \text{if } k = 1, \\ (\Pi^\nabla_{k,E}(v), 1)_E &= (v, 1)_E, && \text{if } k > 1. \end{aligned}$$

- $L^2(E)$*-orthogonal projection operator* $\Pi^0_{k,E} : L^2(E) \to \mathbb{P}_k(E)$ with $k \in \mathbb{N}$, defined as

$$(\Pi^0_{k,E}(v), p)_E = (v, p)_E, \quad \forall p \in \mathbb{P}_k(E), \;\; v \in L^2(E).$$

- $L^2(E)$*-orthogonal projection operators of derivatives* $\Pi^0_{k-1,E}\frac{\partial}{\partial x}$, $\Pi^0_{k-1,E}\frac{\partial}{\partial y} : H^1(E) \to \mathbb{P}_{k-1}(E)$ with $k \in \mathbb{N}$, defined as

$$\begin{aligned} \Big(\Pi^0_{k-1,E}\frac{\partial v}{\partial x}, p\Big)_E &= \Big(\frac{\partial v}{\partial x}, p\Big)_E, \\ \Big(\Pi^0_{k-1,E}\frac{\partial v}{\partial y}, p\Big)_E &= \Big(\frac{\partial v}{\partial y}, p\Big)_E, \end{aligned} \tag{9}$$

for all $p \in \mathbb{P}_{k-1}(E), v \in L^2(E)$.

Moreover, we denote by Π_k^∇, Π_k^0 and $\Pi_{k-1}^0 \frac{\partial}{\partial x}, \Pi_{k-1}^0 \frac{\partial}{\partial y}$, the global projectors that are defined elementwise by the corresponding local ones above. To ensure that the projection operators defined above are all computable, we use the definition of the local element space introduced in [4].

Let $k \geq 1$ be the order of the virtual element method we want to use. We define

$$\mathbb{B}_k(\partial E) := \Big\{ v \in C^0(\partial E) : v_{|e} \in \mathbb{P}_k(e),\ \forall e \in \mathcal{E}_{\delta,E} \Big\},$$

and the *local virtual element space* $\mathcal{V}_\delta^{k,E}$ as

$$\mathcal{V}_\delta^{k,E} := \Big\{ v \in H^1(E) : v_{|\partial E} \in \mathbb{B}_k(\partial E),\ \Delta v_{|E} \in \mathbb{P}_k(E), \\ (v,p)_E = (\Pi_{k,E}^\nabla(v), p)_E,\ \forall p \in \mathbb{P}_k(E)/\mathbb{P}_{k-2}(E) \Big\}.$$

For $E \subset \mathbb{R}^2$, we select the set of scaled monomials $\mathcal{M}_k(E)$ as a basis for the local polynomial space $\mathbb{P}_k(E)$

$$\mathcal{M}_k(E) := \Big\{ m \mid m(x,y) = \frac{(x-x_E)^{\alpha_x}(y-y_E)^{\alpha_y}}{\delta_E^{\alpha_x+\alpha_y}}, 0 \leq \alpha_x + \alpha_y \leq k \Big\},$$

where (x_E, y_E) is the centroid of E. It can be easily verified that the elements of $\mathcal{M}_k(E)$ form a basis for the space of polynomials of degree less or equal to k on E and that the dimension N_k of $\mathcal{M}_k(E)$ is $N_k := \dim(\mathcal{M}_k(E)) = \frac{(k+1)(k+2)}{2}$.

$\mathbb{P}_k(E)/\mathbb{P}_{k-2}(E)$ appearing in the definition of the local virtual element space will denote the linear space spanned by the scaled monomials of degree k and $k-1$ on E.

Given $v \in \mathcal{V}_\delta^{k,E}$, we consider the following as *degrees of freedom* in $\mathcal{V}_\delta^{k,E}$:

1. values of v at the vertices of the polygon E;
2. for $k > 1$, the values of v at the $k-1$ internal points of the $k+1$ points of the Gauss-Lobatto quadrature rule on each edge e;
3. for $k > 1$, the momentum up to order $k-2$ of v in E, i.e., $\frac{1}{|E|}\int_E v\ m\ \mathrm{d}\mathbf{x}, \quad m \in \mathcal{M}_{k-2}(E)$.

The dimension of $\mathcal{V}_\delta^{k,E}$ is equal to the number of degrees of freedom (1)-(3), i.e., $N_{dof}^{k,E} := \dim(\mathcal{V}_\delta^{k,E}) = N_{V,E} + N_{V,E}(k-1) + N_{k-2}$, where $N_{V,E}$ is the number of vertices of E and $N_{k-2} = \dim(\mathcal{M}_{k-2}(E)) = \frac{k(k-1)}{2}$. Moreover, it can be proved that these degrees of freedom are unisolvent in $\mathcal{V}_\delta^{k,E}$ [4].

The local virtual element space possess the following well-established properties:

1. for each element $E \in \mathcal{T}_\delta$, $\mathbb{P}_k(E) \subseteq \mathcal{V}_\delta^{k,E}$ as a subspace and this guarantees good approximation properties;
2. for each element $E \in \mathcal{T}_\delta$ and for each $v \in \mathcal{V}_\delta^{k,E}$, the degrees of freedom are sufficient in order to compute all the projection operators previously defined ([4], [5]).

The *global virtual element space* is constructed as a finite subspace of the infinite dimensional space $H_0^1(\Omega)$ and it is obtained from the local spaces $\mathcal{V}_\delta^{k,E}$ as follows

$$V_\delta^k := \Big\{ v \in H_0^1(\Omega) : v_{|E} \in \mathcal{V}_\delta^{k,E},\ \forall E \in \mathcal{T}_\delta \Big\}.$$

We select two distinct virtual element spaces for p_n and for S_w. We denote as k_p and as k_S the selected values of the integer k for the pressure and the saturation, respectively. As a consequence, the related global virtual element spaces are denoted by $V_\delta^{k_p}$ and $V_\delta^{k_S}$, respectively. However, in the numerical examples, we will always consider $k_p = k_S = k$.

Furthermore, we introduce the operator $\mathrm{dof}_i^k : \mathcal{V}_\delta^{k,E} \to \mathbb{R}$ defined as $\mathrm{dof}_i^k(v) :=$ i-th degree of freedom of $v \in \mathcal{V}_\delta^{k,E}$, for $i \in \{1, ..., N_{dof}^{k,E}\}$.

Now, we introduce suitable discrete forms constructed elementwise using the projection operators previously defined.

The fully discrete virtual element variational formulation of (8) reads:

Given $S_{w_\delta}(t^{n+1}, \hat{k}+1) \in V_\delta^{k_S}$*, find* $p_{n_\delta}(t^{n+1}, \hat{k}+1) \in V_\delta^{k_p}$*,* $\hat{k} \geq 0$*, such that the following holds true* $\forall v_{p_\delta} \in V_\delta^{k_p}$

$$a_\delta(S_{w_\delta}(t^{n+1}, \hat{k}+1); p_{n_\delta}(t^{n+1}, \hat{k}+1), v_{p_\delta}) = F^P_{t^{n+1},\delta}(S_{w_\delta}(t^{n+1}, \hat{k}+1), v_{p_\delta}), \tag{10}$$

with

$$F^P_{t,\delta}(z, w) := (q(t), \Pi^0_{k_p} w)_\Omega - b_\delta(z, w) - g_\delta(z, w).$$

$a_\delta(\cdot;\cdot,\cdot)$ is the global forms bilinear and symmetric in its second and third arguments defined as the sum of elementwise contributions $a^E_\delta(\cdot;\cdot,\cdot)$, with $E \in \mathcal{T}_\delta$. Moreover, also $b_\delta(\cdot,\cdot)$ and $g_\delta(\cdot,\cdot)$ are defined as the sum of elementwise contributions $b^E_\delta(\cdot,\cdot)$ and $g^E_\delta(\cdot,\cdot)$, respectively, with $E \in \mathcal{T}_\delta$. All these local contributions must be defined in order to be computable and must approximate the corresponding exact local form in the way that is specified in what follows.

The local form $a^E_\delta(\cdot;\cdot,\cdot)$ must be bilinear and symmetric in its second and third argument and it must satisfy polynomial consistency and stability that are defined as follows.

- *Polynomial consistency*: for all $E \in \mathcal{T}_\delta$, if either $p \in \mathbb{P}_{k_p}(E)$ or $v \in \mathbb{P}_{k_p}(E)$ the local form $a^E_\delta(\cdot;\cdot,\cdot)$ becomes $\forall z \in \mathcal{V}_\delta^{k_S,E}$

$$a^E_\delta(z; p, v) = \int_E [\Pi^0_{k_p-1,E}\nabla p]^T \ \boldsymbol{K}\lambda(\Pi^0_{k_S,E} z)\ [\Pi^0_{k_p-1,E}\nabla v]\ \mathrm{d}\mathbf{x}.$$

- *Stability*: there exist constants α_* and α^* independent of δ and the mesh element E such that for all $v \in \mathcal{V}_\delta^{k_p,E}, z \in \mathcal{V}_\delta^{k_S,E}$

$$\alpha_* a^E(z; v, v) \leq a^E_\delta(z; v, v) \leq \alpha^* a^E(z; v, v),$$

  where $a^E(\cdot;\cdot,\cdot)$ is the exact local form corresponding to the global form $a(\cdot;\cdot,\cdot)$.

We point out that the above requirements are similar to those introduced for the linear setting in [5] or [7], but with the fractional flow λ evaluated in the polynomial projection $\Pi^0_{k_S,E}$ of the argument as done in [28]. It can be proved that the symmetry and the stability assumptions imply the continuity in $V_\delta^{k_p}$ of the form a_δ.

In particular, we choose the following expression for the local form a^E_δ

$$a^E_\delta(z; v, w) := \int_E [\Pi^0_{k_p-1,E}\nabla v]^T \ \boldsymbol{K}\lambda(\Pi^0_{k_S,E} z)\ [\Pi^0_{k_p-1,E}\nabla w]\ \mathrm{d}\mathbf{x} + S^E\Big(z; (I - \Pi^\nabla_{k_p,E})v, (I - \Pi^\nabla_{k_p,E})w\Big), \tag{11}$$

where S^E is an admissible stabilizing form, i.e., a computable bilinear form in its second and third arguments $\mathcal{V}_\delta^{k_S,E} \times \mathcal{V}_\delta^{k_p,E}/\mathbb{P}_{k_p}(E) \times \mathcal{V}_\delta^{k_p,E}/\mathbb{P}_{k_p}(E) \to \mathbb{R}$ that is symmetric and positive definite in its second and third arguments and satisfies $c_0 a^E(z; v, v) \leq S^E(z; v, v) \leq c_1 a^E(z; v, v)$, $\forall z \in \mathcal{V}_\delta^{k_S,E}$, $\forall v \in \mathcal{V}_\delta^{k_p,E}/\mathbb{P}_{k_p}(E)$, for some positive constants c_0, c_1 independent of E and δ. In particular, we choose the following expression for the S^E stabilizing form

$$S^E\Big(z; (I - \Pi^\nabla_{k_p,E})v, (I - \Pi^\nabla_{k_p,E})w\Big) := ||\boldsymbol{K}\lambda(\Pi^0_{k_S,E} z)||_{L^\infty(E)} \cdot \sum_{l=1}^{N^{k_p,E}_{dof}} \mathrm{dof}^{k_p}_l\Big((I - \Pi^\nabla_{k_p,E})v\Big)\mathrm{dof}^{k_p}_l\Big((I - \Pi^\nabla_{k_p,E})w\Big),$$

where I denotes the identity operator.

It can be easily verified that this definition of a^E_δ satisfies the stability condition above. In particular, we point out that the first member of (11) ensures the polynomial consistency of the local form, while the second one the stability.

Remark. In the FEM, we expect that a scheme of order greater or equal to k will be able to reproduce exactly every polynomial solution of degree up to k in space, i.e., the method is consistent. This holds true in general, whatever are the coefficients (even non-polynomial functions). For the VEM this is not always true for general coefficients. Indeed, there is an additional inconsistency error to take into account due to the introduction of the L^2-orthogonal projection operators of derivatives (9) in the definition of the form (11). Consequently, for general coefficients, even when the pressure solution is a polynomial, the discrete form (11) does not coincide with the continuous form $a^E(\cdot;\cdot,\cdot)$. The only exception is the VEM of order $k=1$ on a triangular mesh. This is the reason why we defined polynomial consistency as explained before following [7] and [28], rather than [2] or [4]. Furthermore, in the practical implementation, the non-constant coefficients must be approximated using numerical quadrature. Consequently, the polynomial consistency property introduced before holds true only approximately.

The terms $b_\delta^E(\cdot,\cdot)$ and $g_\delta^E(\cdot,\cdot)$ are defined as follows

$$b_\delta^E(z,w) := -\int_E [\Pi^0_{k_S-1,E}\nabla z]^T\ \boldsymbol{K}\lambda_w(\Pi^0_{k_S,E}z)\frac{dp_c(\Pi^0_{k_S,E}z)}{dS_w}\ [\Pi^0_{k_p-1,E}\nabla w]\ \mathrm{d}\mathbf{x},$$
$$g_\delta^E(z,w) := -\int_E \boldsymbol{g}^T\ \boldsymbol{K}\Big(\lambda_w(\Pi^0_{k_S,E}z)\rho_w + \lambda_n(\Pi^0_{k_S,E}z)\rho_n\Big)[\Pi^0_{k_p-1,E}\nabla w]\ \mathrm{d}\mathbf{x}.$$

Now, we focus on variational formulation (7) related to the saturation S_w. The fully discrete virtual element variational formulation of the saturation equation reads:

Given $S_{w_\delta}(t^n)$, $S_{w_\delta}(t^{n+1},\hat{k}) \in V_\delta^{k_S}$ *and* $p_{n_\delta}(t^n)$, $p_{n_\delta}(t^{n+1},\hat{k}) \in V_\delta^{k_p}$, *find* $S_{w_\delta}(t^{n+1},\hat{k}+1) \in V_\delta^{k_S}$, $\hat{k}\geq 0$, *such that the following relation holds true* $\forall v_{S_\delta} \in V_\delta^{k_S}$

$$\begin{aligned} &c_\delta(\delta S_{w_\delta}(t^{n+1},\hat{k}+1), v_{S_\delta}) + \frac{\Delta t}{2}\tilde{F}_\delta^S(S_{w_\delta}(t^{n+1},\hat{k}), \delta S_{w_\delta}(t^{n+1},\hat{k}+1), p_{n_\delta}(t^{n+1},\hat{k}), v_{S_\delta}) \qquad (12)\\ &= -c_\delta(S_{w_\delta}(t^{n+1},\hat{k}), v_{S_\delta}) + \frac{\Delta t}{2}F^S_{t^{n+1},\delta}(S_{w_\delta}(t^{n+1},\hat{k}), S_{w_\delta}(t^{n+1},\hat{k}), p_{n_\delta}(t^{n+1},\hat{k}), v_{S_\delta})\\ &+ c_\delta(S_{w_\delta}(t^n), v_{S_\delta}) + \frac{\Delta t}{2}F^S_{t^n,\delta}(S_{w_\delta}(t^n), S_{w_\delta}(t^n), p_{n_\delta}(t^n), v_{S_\delta}), \end{aligned}$$

where $S_{w_\delta}(t^{n+1},0) := S_{w_\delta}(t^n)$, $p_{n_\delta}(t^{n+1},0) := p_{n_\delta}(t^n)$ *and*

$$F^S_{t,\delta}(z_1,z_2,v,w) := (q_w(t),\Pi^0_{k_S}w)_\Omega - d_\delta(z_1;z_2,w) - e_\delta(z_1,v,w) - f_\delta(z_1,w),$$
$$\tilde{F}^S_\delta(z_1,z_2,v,w) := d_\delta(z_1;z_2,w) + l_\delta(z_1;z_2,w) + m_\delta(z_1;v;z_2,w) + n_\delta(z_1;z_2,w).$$

The form $c_\delta(\cdot,\cdot)$ is a global symmetric and bilinear form and $d_\delta(\cdot;\cdot,\cdot)$ is a global form symmetric and bilinear in its second and third arguments defined as the sum of the elementwise contributions $c_\delta^E(\cdot,\cdot)$ and $d_\delta^E(\cdot;\cdot,\cdot)$, respectively, with $E\in\mathcal{T}_\delta$. Moreover, also $e_\delta(\cdot;\cdot,\cdot)$, $f_\delta(\cdot,\cdot)$, $l(\cdot;\cdot,\cdot)$, $m(\cdot;\cdot;\cdot,\cdot)$ and $n(\cdot;\cdot,\cdot)$ are defined as the sum of the elementwise contributions $e_\delta^E(\cdot;\cdot,\cdot)$, $f_\delta^E(\cdot,\cdot)$, $l_\delta^E(\cdot;\cdot,\cdot)$, $m_\delta^E(\cdot;\cdot;\cdot,\cdot)$ and $n_\delta^E(\cdot;\cdot,\cdot)$, respectively, with $E\in\mathcal{T}_\delta$. All the local forms must be computable and they must approximate the corresponding exact local forms. The local form $c_\delta^E(\cdot,\cdot)$ is bilinear and symmetric and the local form $d_\delta^E(\cdot;\cdot,\cdot)$ must be bilinear and symmetric in its second and third argument. Both of them must satisfy polynomial consistency and stability that are defined as follows.

- *Polynomial consistency*: for all $E\in\mathcal{T}_\delta$, if either $p\in\mathbb{P}_{k_S}(E)$ or $v\in\mathbb{P}_{k_S}(E)$, the local forms $c_\delta^E(\cdot,\cdot)$ and $d_\delta^E(\cdot,\cdot;\cdot)$ becomes $\forall z\in\mathcal{V}_\delta^{k_S,E}$

$$c_\delta^E(p,v) = \int_E \Phi\ \Pi^0_{k_S,E}p\ \Pi^0_{k_S,E}v\ \mathrm{d}\mathbf{x},$$
$$d_\delta^E(z;p,v) = -\int_E [\Pi^0_{k_S-1,E}\nabla p]^T\boldsymbol{K}\lambda_w(\Pi^0_{k_S}z)\frac{dp_c(\Pi^0_{k_S}z)}{dz}[\Pi^0_{k_S-1,E}\nabla v]\ \mathrm{d}\mathbf{x}.$$

- *Stability*: there exist constants c_*, c^*, d_* and d^* independent of δ and the mesh element E such that for all $v,z\in\mathcal{V}_\delta^{k_S,E}$

$$c_* c^E(v,v) \leq c_\delta^E(v,v) \leq c^* c^E(v,v),$$

$$d_* d^E(z;v,v) \leq d_\delta^E(z;v,v) \leq d^* d^E(z;v,v),$$

where $d^E(\cdot;\cdot,\cdot)$ and $c^E(\cdot,\cdot)$ are the exact local forms corresponding to the global form $d(\cdot;\cdot,\cdot)$ and $c(\cdot,\cdot)$, respectively.

In particular, we choose the following expression for the local form c_δ^E

$$c_\delta^E(v,w) := \int_E \Phi \Pi^0_{k_S,E} v \ \Pi^0_{k_S,E} w \ \mathrm{d}\mathbf{x} + M^E\Big((I-\Pi^0_{k_S,E})v, (I-\Pi^0_{k_S,E})w\Big), \tag{13}$$

where M^E is a stabilizing bilinear form, i.e., a computable bilinear form $\mathcal{V}_\delta^{k_S,E}/\mathbb{P}_{k_S}(E) \times \mathcal{V}_\delta^{k_S,E}/\mathbb{P}_{k_S}(E) \to \mathbb{R}$ symmetric and positive definite that satisfies $c_o c^E(v,v) \leq M^E(v,v) \leq c_1 c^E(v,v), \quad \forall v \in \mathcal{V}_\delta^{k_S,E}/\mathbb{P}_{k_S(E)}$, for some positive constants c_0, c_1 independent of E and δ. We select the following expression for the M^E stabilizing form

$$M^E\Big((I-\Pi^0_{k_S,E})v, (I-\Pi^0_{k_S,E})w\Big) := ||\Phi||_{L^\infty(E)} \delta_E^2 \sum_{l=1}^{N_{dof}^{k_S,E}} \mathrm{dof}_l^{k_S}\Big((I-\Pi^0_{k_S,E})v\Big)\mathrm{dof}_l^{k_S}\Big((I-\Pi^0_{k_S,E})w\Big).$$

Moreover, we choose the following expression for the local form d_δ^E

$$\begin{aligned} &d_\delta^E(z_1;z_2,w) := \\ &-\int_E [\Pi^0_{k_S-1,E}\nabla z_2]^T \ \boldsymbol{K}\lambda_w(\Pi^0_{k_S,E}z_1)\frac{dp_c(\Pi^0_{k_S,E}z_1)}{dS_w}\ [\Pi^0_{k_S-1,E}\nabla w]\ \mathrm{d}\mathbf{x} \\ &+ D^E\Big(z_1; (I-\Pi^\nabla_{k_S,E})z_2, (I-\Pi^\nabla_{k_S,E})w\Big), \end{aligned} \tag{14}$$

where D^E is a stabilizing bilinear form in its second and third arguments, that is, a computable bilinear form $\mathcal{V}_\delta^{k_S,E} \times \mathcal{V}_\delta^{k_S,E}/\mathbb{P}_{k_S}(E) \times \mathcal{V}_\delta^{k_S,E}/\mathbb{P}_{k_S}(E) \to \mathbb{R}$ symmetric and positive definite in its second and third argument that satisfies $d_0 d^E(z;v,v) \leq D^E(z;v,v) \leq d_1 d^E(z;v,v)$, $\forall z \in \mathcal{V}_\delta^{k_S,E}$, $\forall v \in \mathcal{V}_\delta^{k_S,E}/\mathbb{P}_{k_S}(E)$ and for some positive constants d_0, d_1 independent of E and δ. We choose the following expression for the D^E stabilizing form

$$\begin{aligned} &D^E\Big(z_1; (I-\Pi^\nabla_{k_S,E})z_2, (I-\Pi^\nabla_{k_S,E})w\Big) := \\ &\Big|\Big|\boldsymbol{K}\lambda_w(\Pi^0_{k_S,E}z_1)\frac{dp_c(\Pi^0_{k_S,E}z_1)}{dS_w}\Big|\Big|_{L^\infty(E)} \sum_{l=1}^{N_{dof}^{k_S,E}} \mathrm{dof}_l^{k_S}\Big((I-\Pi^\nabla_{k_S,E})z_2\Big)\mathrm{dof}_l^{k_p}\Big((I-\Pi^\nabla_{k_S,E})w\Big). \end{aligned}$$

It can be easily verified that the definition of c_δ^E and d_δ^E satisfy the consistency and the stability conditions above. In particular, the first members of (13) and (14) ensure polynomial consistency of the forms, whereas the second members the stability. For $e_\delta^E(\cdot;\cdot,\cdot)$, $f_\delta^E(\cdot,\cdot)$, $l_\delta^E(\cdot;\cdot,\cdot)$, $m_\delta^E(\cdot;\cdot;\cdot,\cdot)$ and $n_\delta^E(\cdot;\cdot,\cdot)$ we propose the following local approximations

$$\begin{aligned} e_\delta^E(z_1;v,w) &:= \int_E [\Pi^0_{k_S-1,E}\nabla v]^T \ \boldsymbol{K}\lambda_w(\Pi^0_{k_S,E}z_1)\ [\Pi^0_{k_S-1,E}\nabla w]\ \mathrm{d}\mathbf{x}, \\ f_\delta^E(z_1,w) &:= -\int_E \boldsymbol{g}^T \ \boldsymbol{K}\lambda_w(\Pi^0_{k_S,E}z_1)\rho_w\ [\Pi^0_{k_S-1,E}\nabla w]\ \mathrm{d}\mathbf{x}, \\ l_\delta^E(z_1;z_2,w) &:= -\int_E z_2\ [\Pi^0_{k_S-1,E}\nabla z_1]^T \boldsymbol{K} b(\Pi^0_{k_S,E}z_1)[\Pi^0_{k_S-1,E}\nabla w]\ \mathrm{d}\mathbf{x}, \\ m_\delta^E(z_1;v;z_2,w) &:= \int_E z_2\ [\Pi^0_{k_p-1,E}\nabla v]^T \boldsymbol{K} r(\Pi^0_{k_S,E}z_1)\ [\Pi^0_{k_S-1,E}\nabla w]\ \mathrm{d}\mathbf{x}, \\ n_\delta^E(z_1;z_2,w) &:= -\int_E z_2\ \boldsymbol{g}^T \boldsymbol{K} r(\Pi^0_{k_S,E}z_1)\rho_w\ [\Pi^0_{k_S-1,E}\nabla w]\ \mathrm{d}\mathbf{x}. \end{aligned}$$

5 Resolution algorithm

In this section we propose a matrix-based approach to the problem presented above. In particular, we introduce the local matrices that need to be assembled as well as the local contributions to the right-hand side. To this aim we introduce a basis v_{p_α} of $\mathcal{V}_\delta^{k_p,E}$ with $\alpha \in \{1,...,N_{dof}^{k_p,E}\}$ and a basis v_{S_l} of $\mathcal{V}_\delta^{k_S,E}$ with $l \in \{1,...,N_{dof}^{k_S,E}\}$, so that for all $v_{p_\delta} \in \mathcal{V}_\delta^{k_p,E}$ and for all $v_{S_\delta} \in \mathcal{V}_\delta^{k_S,E}$ we have

$$v_{p_\delta} = \sum_{\alpha=1}^{N_{dof}^{k_p,E}} \text{dof}_\alpha^{k_p}(v_{p_\delta}) v_{p_\alpha}, \quad v_{S_\delta} = \sum_{l=1}^{N_{dof}^{k_S,E}} \text{dof}_l^{k_S}(v_{S_\delta}) v_{S_l}.$$

In particular, we choose Lagrangian basis functions with respect to the degrees of freedom.

To begin with, we focus on variational formulation (10). We have to solve the following linear system of equations

$$\begin{aligned}\mathbf{A}(S_{w_\delta}(t^{n+1},\hat{k}+1))\ \mathbf{Dof_p}(p_{n_\delta}(t^{n+1},\hat{k}+1)) = &-\mathbf{B}(S_{w_\delta}(t^{n+1},\hat{k}+1))\mathbf{Dof_S}(S_{w_\delta}(t^{n+1},\hat{k}+1)) \\ &- \mathbf{g}(S_{w_\delta}(t^{n+1},\hat{k}+1)) + \mathbf{b}(t^{n+1}). \end{aligned} \tag{15}$$

$\mathbf{A}(z) \in \mathbb{R}^{N_{dof}^{k_p},N_{dof}^{k_p}}$ and $\mathbf{B}(z) \in \mathbb{R}^{N_{dof}^{k_p},N_{dof}^{k_S}}$ are the global matrices of the problem assembled from the following local matrices $\mathbf{A}_E(z) \in \mathbb{R}^{N_{dof}^{k_p,E},N_{dof}^{k_p,E}}$ and $\mathbf{B}_E(z) \in \mathbb{R}^{N_{dof}^{k_p,E},N_{dof}^{k_S,E}}$, respectively, defined as

$$\begin{aligned}\mathbf{A}_{E_{\alpha,j}}(z) &:= (\boldsymbol{K}\lambda(\Pi^0_{k_S,E}z)\ \Pi^0_{k_p-1,E}\nabla v_{p_j}, \Pi^0_{k_p-1,E}\nabla v_{p_\alpha})_E \\ &\quad + S^E\Big(z; (I-\Pi^0_{k_p-1,E})v_{p_j}, (I-\Pi^0_{k_p-1,E})v_{p_\alpha}\Big), \\ \mathbf{B}_{E_{\alpha,l}}(z) &:= -\Big(\boldsymbol{K}\lambda_w(\Pi^0_{k_S,E}z)\ \frac{dp_c(\Pi^0_{k_S,E}z)}{dS_w}\ \Pi^0_{k_S-1,E}\nabla v_{S_l}, \Pi^0_{k_p-1,E}\nabla v_{p_\alpha}\Big)_E,\end{aligned}$$

with $\alpha, j \in \{1,...,N_{dof}^{k_p,E}\}$ and $l \in \{1,...,N_{dof}^{k_S,E}\}$. $\mathbf{g}(z) \in \mathbb{R}^{N_{dof}^{k_p}}$ is the global vector assembled from the local vector $\mathbf{g}_E(z) \in \mathbb{R}^{N_{dof}^{k_p,E}}$

$$\mathbf{g}_{E_\alpha}(z) := -\Big(\boldsymbol{K}\big(\lambda_w(\Pi^0_{k_S,E}z)\rho_w + \lambda_n(\Pi^0_{k_S,E}z)\rho_n\big)\ \boldsymbol{g}, \Pi^0_{k_p-1,E}\nabla v_{p_\alpha}\Big)_E,$$

with $\alpha \in \{1,...,N_{dof}^{k_p,E}\}$. $\mathbf{b}(t) \in \mathbb{R}^{N_{dof}^{k_p}}$ is the global vector assembled from the local vector $\mathbf{b}_E(t) \in \mathbb{R}^{N_{dof}^{k_p,E}}$

$$\mathbf{b}_{E_\alpha}(t) := (q(t), \Pi^0_{k_p,E}v_{p_\alpha})_E,$$

with $\alpha \in \{1,...,N_{dof}^{k_p,E}\}$. Finally, $\mathbf{Dof_p}(z) \in \mathbb{R}^{N_{dof}^{k_p}}$ and $\mathbf{Dof_S}(z) \in \mathbb{R}^{N_{dof}^{k_S}}$ are the global vectors of the degrees of freedom of p_{n_δ} and S_{w_δ}, respectively, with respect to the VEM basis. They are assembled starting from the local vectors $\mathbf{Dof_{p,E}}(z) \in \mathbb{R}^{N_{dof}^{k_p,E}}$ and $\mathbf{Dof_{S,E}}(z) \in \mathbb{R}^{N_{dof}^{k_S,E}}$

$$\Big(\mathbf{Dof_{p,E}}(z)\Big)_j := \text{dof}_j^{k_p}(z), \quad \Big(\mathbf{Dof_{S,E}}(z)\Big)_l := \text{dof}_l^{k_S}(z),$$

with $j \in \{1,...,N_{dof}^{k_p,E}\}$ and $l \in \{1,...,N_{dof}^{k_S,E}\}$.

Now we focus on variational formulation (12). The linearization via Newton method involves the iterative solution of the following linear system of equations

$$\begin{aligned}&\mathbf{J}(S_{w_\delta}(t^{n+1},\hat{k}), p_{n_\delta}(t^{n+1},\hat{k}))\mathbf{\Delta Dof_S}(S_{w_\delta}(t^{n+1},\hat{k}+1)) = \\ &-\mathbf{F}_{t^n,t^{n+1}}(S_{w_\delta}(t^{n+1},\hat{k}), p_{n_\delta}(t^{n+1},\hat{k}), S_{w_\delta}(t^n), p_{n_\delta}(t^n)),\end{aligned} \tag{16}$$

where $\mathbf{\Delta Dof_S}(S_{w_\delta}(t,\hat{k}+1)) := \mathbf{Dof_S}(S_{w_\delta}(t,\hat{k}+1)) - \mathbf{Dof_S}(S_{w_\delta}(t,\hat{k})) \in \mathbb{R}^{N_{dof}^{k_S}}$ and $\mathbf{J}(z) \in \mathbb{R}^{N_{dof}^{k_S},N_{dof}^{k_S}}$ is the global Jacobian matrix assembled from the local Jacobian matrix $\mathbf{J}_E(z) \in \mathbb{R}^{N_{dof}^{k_S,E},N_{dof}^{k_S,E}}$

$$\mathbf{J}_E(z,w) := \mathbf{C}_E + \frac{\Delta t}{2}\Big(\mathbf{L}_E(z) + \mathbf{D}_E(z) + \mathbf{M}_E(z,w) + \mathbf{N}_E(z)\Big),$$

and $\mathbf{F}_{t^n,t^{n+1}}(z_1,w_1,z_2,w_2) \in \mathbb{R}^{N_{dof}^{k_S}}$ is the global vector assembled from the local vector $\mathbf{F}_{t^n,t^{n+1},E}(z_1,w_1,z_2,w_2) \in \mathbb{R}^{N_{dof}^{k_S,E}}$ defined as follows

$$\begin{aligned}
&\mathbf{F}_{t^n,t^{n+1},E}(z_1,w_1,z_2,w_2) := \\
&\mathbf{C}_E\Big(\mathbf{Dof}_{\mathbf{S},E}(z_1)-\mathbf{Dof}_{\mathbf{S},E}(z_2)\Big)+\frac{\Delta t}{2}\Big(\mathbf{D}_E(z_1)\mathbf{Dof}_{\mathbf{S},E}(z_1)+\mathbf{E}_E(z_1)\mathbf{Dof}_{\mathbf{p},E}(w_1)+\mathbf{f}_E(z_1)\\
&-\mathbf{d}_E(t^{n+1})\Big)+\frac{\Delta t}{2}\Big(\mathbf{D}_E(z_2)\mathbf{Dof}_{\mathbf{S},E}(z_2)+\mathbf{E}_E(z_2)\mathbf{Dof}_{\mathbf{p},E}(w_2)+\mathbf{f}_E(z_2)-\mathbf{d}_E(t^n)\Big).
\end{aligned}$$

where

$$\begin{aligned}
\mathbf{C}_{E_{\beta,l}} &:= \Big(\Phi\Pi^0_{k_S,E}v_{S_l},\Pi^0_{k_S,E}v_{S_\beta}\Big)_E + M^E\Big((I-\Pi^0_{k_S,E})v_{S_l},(I-\Pi^0_{k_S,E})v_{S_\beta})\Big),\\
\mathbf{D}_{E_{\beta,l}}(z) &:= -\Big(\boldsymbol{K}\lambda_w(\Pi^0_{k_S,E}z)\frac{dp_c(\Pi^0_{k_S,E}z)}{dS_w}\Pi^0_{k_S-1,E}\nabla v_{S_l},\Pi^0_{k_S-1,E}\nabla v_{S_\beta}\Big)_E\\
&\quad + D^E\Big(z;(I-\Pi^\nabla_{k_S,E})v_{S_l},(I-\Pi^\nabla_{k_S,E})v_{S_\beta})\Big),\\
\mathbf{E}_{E_{\beta,j}}(z) &:= \Big(\boldsymbol{K}\lambda_w(\Pi^0_{k_S,E}z)\ \Pi^0_{k_p-1}\nabla v_{p_j},\Pi^0_{k_S-1,E}\nabla v_{S_\beta}\Big)_E,\\
\mathbf{L}_{E_{\beta,l}}(z) &:= -\Big(\Pi^0_{k_S,E}v_{S_l}\boldsymbol{K}\ b(\Pi^0_{k_S,E}z)\Pi^0_{k_S-1,E}\nabla z,\Pi^0_{k_S-1,E}\nabla v_{S_\beta}\Big)_E,\\
\mathbf{M}_{E_{\beta,l}}(z,w) &:= \Big(\Pi^0_{k_S,E}v_{S_l}\boldsymbol{K}\ r(\Pi^0_{k_S,E}z)\Pi^0_{k_p-1,E}\nabla w,\Pi^0_{k_S-1,E}\nabla v_{S_\beta}\Big)_E,\\
\mathbf{N}_{E_{\beta,l}}(z) &:= -\Big(\Pi^0_{k_S,E}v_{S_l}\ \boldsymbol{K}\ r(\Pi^0_{k_S,E}z)\ \rho_w\boldsymbol{g},\Pi^0_{k_S-1}\nabla v_{S_\beta}\Big)_E,\\
\mathbf{f}_{E_\beta}(z) &:= -\Big(\boldsymbol{K}\lambda_w(\Pi^0_{k_S,E}z)\rho_w\boldsymbol{g},\Pi^0_{k_S-1}\nabla v_{S_\beta}\Big)_E,\\
\mathbf{d}_{E_\beta}(t) &:= (q_w(t),\Pi^0_{k_S,E}v_{S_\beta})_E,
\end{aligned}$$

where with $\beta,l \in \{1,...,N_{dof}^{k_S,E}\}$ and $j \in \{1...,N_{dof}^{k_p,E}\}$.

In Algorithm 1, we briefly summarize the solution steps for the implementation of the numerical algorithm.

Algorithm 1 Iterative IMPIS-VEM algorithm

- Compute the vector $\mathbf{Dof}_{\mathbf{p}}(S_{w_\delta}(t^0))$ and the matrix $\mathbf{C}$;
- Compute the matrices $\mathbf{A}(S_{w_\delta}(t^0))$ and $\mathbf{B}(S_{w_\delta}(t^0))$, and the vectors $\mathbf{g}(S_{w_\delta}(t^0))$ and $\mathbf{b}(t^0)$.
- Solve the linear system (15) setting $S_{w_\delta}(t^{n+1},\hat{k}) = S_{w_\delta}(t^0)$ and $p_{n_\delta}(t^{n+1},\hat{k}) = p_{n_\delta}(t^0)$ and find the vector $\mathbf{Dof}_{\mathbf{p}}(p_{n_\delta}(t^0))$.
- For $n = 0,\dots,C-1$
  - Compute the matrices $\mathbf{D}(S_{w_\delta}(t^n))$ and $\mathbf{E}(S_{w_\delta}(t^n))$, and the vectors $\mathbf{f}(S_{w_\delta}(t^n))$, $\mathbf{d}(t^n)$ and $\mathbf{d}(t^{n+1})$.
  - For $\hat{k} = 0,1,\dots$ until convergence:
    - Compute the matrices $\mathbf{L}(S_{w_\delta}(t^{n+1},\hat{k})),\mathbf{D}(S_{w_\delta}(t^{n+1},\hat{k}))$, $\mathbf{M}(S_{w_\delta}(t^{n+1},\hat{k}),p_{n_\delta}(t^{n+1},\hat{k}))$, $\mathbf{N}(S_{w_\delta}(t^{n+1},\hat{k}))$ and $\mathbf{E}(S_{w_\delta}(t^{n+1},\hat{k}))$, and the vector $\mathbf{f}(S_{w_\delta}(t^{n+1},\hat{k}))$.
    - Solve the linear system (16) and then compute the vector $\mathbf{Dof}_{\mathbf{S}}(S_{w_\delta}(t^{n+1},\hat{k}+1))$.
    - Compute the matrices $\mathbf{A}(S_{w_\delta}(t^{n+1},\hat{k}+1))$ and $\mathbf{B}(S_{w_\delta}(t^{n+1},\hat{k}+1))$, and the vectors $\mathbf{g}(S_{w_\delta}(t^{n+1},\hat{k}+1))$ and $\mathbf{b}(t^{n+1})$.
    - Solve the linear system (15) and find the vector $\mathbf{Dof}_{\mathbf{p}}(p_{n_\delta}(t^{n+1},\hat{k}+1))$.

Given suitable tolerances tol_1 and tol_2, we require that $||\mathbf{F}_{t^n,t^{n+1}}(S_{w_\delta}(t^{n+1},\hat{k}+1)),p_{n_\delta}(t^{n+1},\hat{k}))||_2 \leq tol_1$ and $||S_{w_\delta}(t^{n+1},\hat{k}+1) - S_{w_\delta}(t^{n+1},\hat{k})||_2 \leq tol_2$ as stopping criterion.

6 Numerical experiments

In this section we analyse the convergence of the method in case the analytical solution is known and for the non-degenerate situation, i.e., when the saturation is a parabolic convection-diffusion equation with respect to S_w. Given the parabolic nature of the coupled non-linear problem (5a)-(5b), we evaluate the spatial discretization error at the end of the time interval through the H^1-norm and the L^2-norm [44]. Moreover, provided that the time integrator error that depends on the size of the time step Δt is sufficiently small, we expect that the H^1-error estimate and the L^2-error estimates for the spatial discretization error related to both the pressure p_{n_δ} and the saturation S_{w_δ} will be similar to those discussed in [5] and [7]. Consequently, we expect an order of convergence with respect to the number of cells $\mathcal{N}_\delta$ of the grid of $O(\mathcal{N}_\delta{}^{-\frac{k_p}{2}})$ and $O(\mathcal{N}_\delta{}^{-\frac{k_p+1}{2}})$ in H^1-norm and in L^2-norm, respectively. In the following numerical experiments we choose exact solutions that linearly depend on time and we try to keep the time discretization error small, so that the discretization error almost coincides with the spatial discretization error.

To test the order of the error in H^1-norm and L^2-norm we consider the virtual element solutions p_{n_δ} and S_{w_δ} of the pressure-saturation formulation for the two-phase flow equation on the unit square $\Omega = (0,1) \times (0,1)$ $[m^2]$ in the time interval $\mathcal{I}_T = [0,1]$ $[s]$, and we compare them with the exact solutions $p_{n_{ex}}$ and $S_{w_{ex}}$ for the pressure of the non-wetting phase and the saturation of the wetting phase, respectively. In particular, we consider the following analytical solutions similar to those proposed in paper [35]

$$p_{n_{ex}}(x,y,t) = 10^5 \cdot tx(1-x)y(1-y) \quad [Pa],$$

$$S_{w_{ex}}(x,y,t) = \frac{1}{2} + tx(1-x)y(1-y) \quad [-].$$

Moreover, we report the physical data of the problem in Table 1. They are taken from [32]. $\mathbf{I}$ denotes the identity matrix.

Porosity	$\Phi = 0.3$ $[-]$
Absolute permeability	$\boldsymbol{K} = 10^{-10} \cdot \mathbf{I}$ $[m^2]$
Residual saturations	$S_{wr} = 0,\ S_{nr} = 0$ $[-]$
Viscosities	$\mu_w = 0.001,\ \mu_n = 0.001$ $[Pa \cdot s]$
Brooks-Corey parameters	$\mu = 1.0$ $[-],\ p_d = 5000$ $[Pa]$

Table 1 Porous medium and fluids data for the problem with analytical solution

Given the exact solutions $p_{n_{ex}}$ and $S_{w_{ex}}$, we insert their analytical expressions as well as all the parameters of the porous medium and of the fluids in the pressure-saturation formulation and we compute the source terms $q(x,y,t)$ and $q_w(x,y,t)$. The gravity term is set equal to zero. The parameters of the porous medium and of the fluids are artificial values selected to be realistic. The function related to the saturation solution has been chosen in order to attain values between 0 and 1 within the given space-time domain, so that it is compatible with the physical requirements. Moreover, we have imposed a magnitude of 10^5 $[Pa]$ to the pressure solution so that it can attain values closer to real ones. Consequently, given the big difference in the orders of magnitude between the pressure and the saturation solutions, we rescale the equations dividing each term by 10^5. Homogeneous Dirichlet boundary conditions both for the pressure and the saturation equations have been imposed.

For the convergence analysis we use four meshes ($\mathcal{T}_{\delta_1}$, $\mathcal{T}_{\delta_2}$, $\mathcal{T}_{\delta_3}$ and $\mathcal{T}_{\delta_4}$) made up of different types of polygonal tessellations. The coarser mesh of each family is shown in Figure 1. The first

type of mesh consists of triangles, the second one of squares, the third one of polygons and the last one of agglomerated cells obtained starting from a triangle grid and agglomerating elements sharing a chosen seed-node. The triangle mesh has been generated by the Triangle library [45] and the polygonal grid by the mesh generator for polygonal elements Polymesher [46]. The square mesh as well as the agglomerated mesh have been implemented by the authors. We compute the errors at $t = 1$ $[s]$ for the four different refinements of each mesh (number of elements: $\mathcal{N}_{\delta_1}$, $\mathcal{N}_{\delta_2}$, $\mathcal{N}_{\delta_3}$ and $\mathcal{N}_{\delta_4}$). At each consecutive refinement the number of elements is selected to be about four time bigger than at the previous refinement. Each refinement is associated to a different time step (time steps: $\Delta t_1, \Delta t_2, \Delta t_3$ and Δt_4). Indeed, we have observed that when we increase either the number of elements of the mesh or the VEM order k we have to decrease the time step in order for the Newton-Raphson scheme to converge. The number of elements for each refinement of the mesh is $\mathcal{N}_{\delta_1} = 36$, $\mathcal{N}_{\delta_2} = 152$, $\mathcal{N}_{\delta_3} = 622$ and $\mathcal{N}_{\delta_4} = 2461$ for the mesh made up of triangles and polygons, $\mathcal{N}_{\delta_1} = 36$, $\mathcal{N}_{\delta_2} = 144$, $\mathcal{N}_{\delta_3} = 625$ and $\mathcal{N}_{\delta_4} = 2500$ for the mesh made up of squares, and $\mathcal{N}_{\delta_1} = 57$, $\mathcal{N}_{\delta_2} = 211$, $\mathcal{N}_{\delta_3} = 902$ and $\mathcal{N}_{\delta_4} = 3527$, for the mesh made up of agglomerated cells. Whereas, the time steps for each refinement are $\Delta t_1 = 0.2$ $[s], \Delta t_2 = 0.1$ $[s], \Delta t_3 = 0.05$ $[s]$ and $\Delta t_4 = 0.025$ $[s]$. For each consecutive refinement, we compute the errors as the norms of the differences between $p_{n_{ex}}$ and the numerical solution p_{n_δ} and between $S_{w_{ex}}$ and the numerical solution S_{w_δ}. Since the VEM solutions p_{n_δ} and S_{w_δ} are not explicitly known inside the elements, we compare $p_{n_{ex}}$ and $S_{w_{ex}}$ with the L^2-orthogonal polynomial projection of p_{n_δ} and S_{w_δ}, i.e., with $\Pi^0_{k_p} p_{n_\delta}$ and $\Pi^0_{k_s} S_{w_\delta}$, respectively. We underline that even if we adopted the Crank-Nicolson scheme that is unconditionally stable for the time discretization, we cannot select an arbitrary time step due to the convergence of the Newton-Raphson scheme. Indeed, the initial guess of the Newton-Raphson method must be sufficiently close to the solution in order to get convergence of the method.

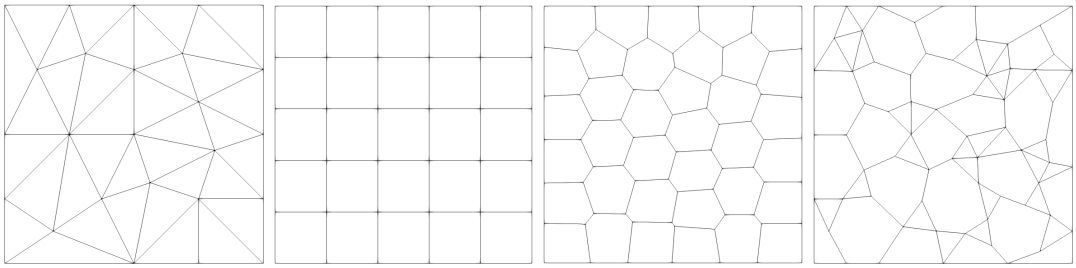

(a) $\mathcal{N}_{\delta_1}$: triangle ($\mathcal{T}_{\delta 1}$) **(b)** $\mathcal{N}_{\delta_1}$: square ($\mathcal{T}_{\delta 2}$) **(c)** $\mathcal{N}_{\delta_1}$: polygon ($\mathcal{T}_{\delta 3}$) **(d)** $\mathcal{N}_{\delta_1}$: agglomerated ($\mathcal{T}_{\delta 4}$)

Figure 1 Meshes

In Figure 2 and in Figure 3 we plot the convergence curves of the error in L^2- and H^1-norm a $t = 1$ $[s]$ in a log-log scale for the VEM of order $k = 1$ and $k = 3$, respectively. The dotted lines having greater slopes are the ones related to the L^2-norm error, whereas the others are the ones related to the H^1-norm error. We can see that the slopes of the dotted lines for both the pressure and the saturation approach the expected convergence rate, i.e., $O({\mathcal{N}_\delta}^{-\frac{k_p}{2}})$ and $O({\mathcal{N}_\delta}^{-\frac{k_p+1}{2}})$ in H^1-norm and in L^2-norm, respectively. Therefore, we conclude that the method behaves as expected and proves stability with respect to the different shapes of the considered polygonal elements.

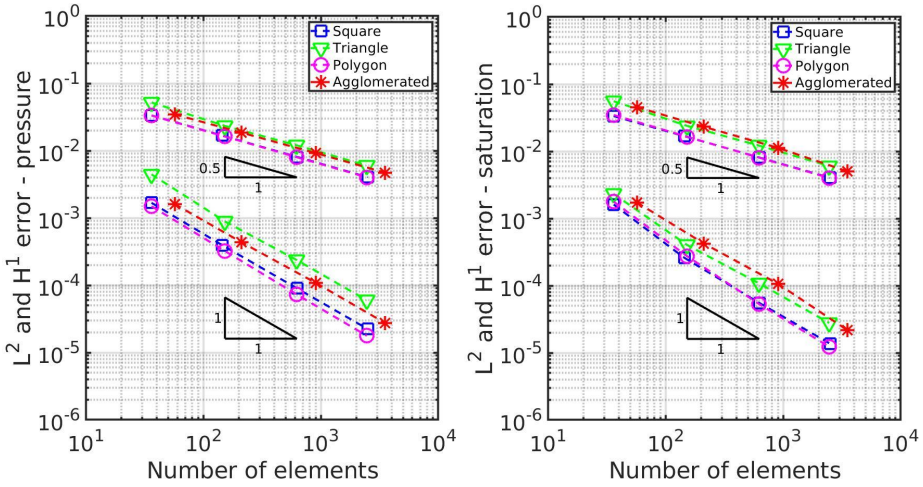

(a) Pressure, $k = 1$, L^2 and H^1 error **(b)** Saturation, $k = 1$, L^2 and H^1 error

Figure 2 Pressure and Saturation, $k = 1$

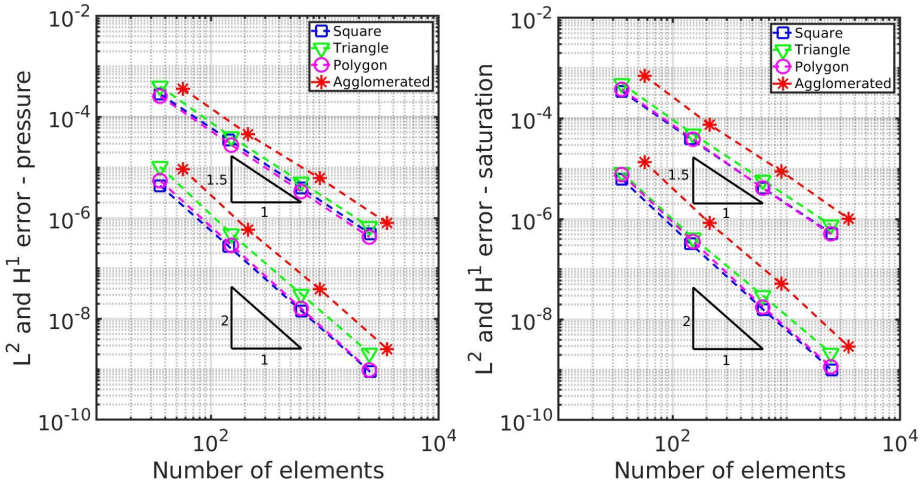

(a) Pressure, $k = 3$, L^2 and H^1 error **(b)** Saturation, $k = 3$, L^2 and H^1 error

Figure 3 Pressure and Saturation, $k = 3$

In Figure 4, we report the number of Newton iterations that are needed in order to satisfy the convergence criteria introduced in Section 5 ($tol_1 = 10^{-20}$, $tol_2 = 10^{-9}$). In particular, in Figure 4a, we show the number of Newton iterations for the meshes having $\mathcal{N}_{\delta_1}$ elements and a time step $\Delta t = 0.2$ $[s]$. Whereas, in Figure 4b we show the number of Newton iterations for the meshes having $\mathcal{N}_{\delta_4}$ elements and a time step $\Delta t = 0.025$ $[s]$. We can see that the number of iterations required does not vary significantly with the shape of the considered mesh elements.

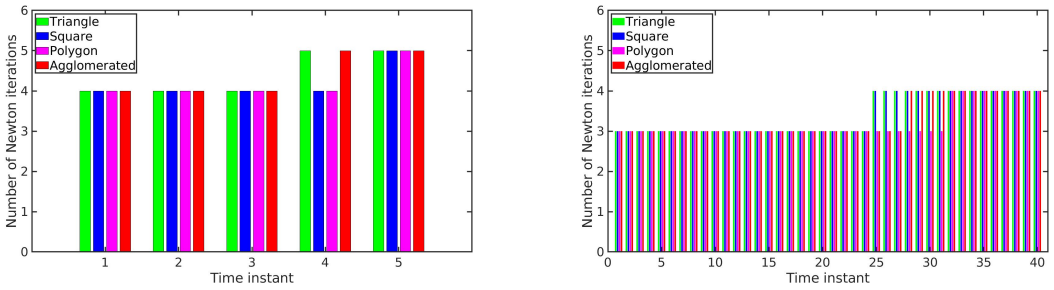

(a) $\mathcal{N}_{\delta_1},\ \Delta t = 0.2\ s$ **(b)** $\mathcal{N}_{\delta_4},\ \Delta t = 0.025\ s$

Figure 4 Newton iterations for the meshes having $\mathcal{N}_{\delta_1}$ and $\mathcal{N}_{\delta_4}$ elements

7 Benchmark problems

The McWhorter and Sunada problem is a well known benchmark problem for the two-phase flow of immiscible fluids in porous media. It involves the flow of two immiscible and incompressible fluids (water and oil, respectively) through a one-dimensional horizontal porous medium representing a reservoir. In particular, the fluid corresponding to the non-wetting phase (oil) is horizontally displaced by the fluid corresponding to the wetting phase (water) that is pumped inside the domain at one side. In the McWhorter and Sunada problem the capillary pressure is taken into account so that the saturation equation turns out to be of parabolic type. In particular, this problem can be either diffusion dominated in case of a *bidirectional flow* (Test Case 1) or possibly convection dominated in case of a *unidirectional flow* (Test Case 2). In what follows, firstly we introduce and describe both the bidirectional and the unidirectional problem and finally we report and discuss the related numerical results. The problems described below are originally mono-dimensional and their domains extend all along the positive part of the real axis. However, since we want to verify the code on a finite bi-dimensional domain $\Omega := (x_i, x_f) \times (y_i, y_f)$, we solve a 2D problem assuming a constant solution on the y direction.

7.1 Test Case 1: Bidirectional flow

McWhorter and Sunada (1990) found a quasi-analytical solution [47] for the two-phase flow equation of immiscible fluids in porous media for a one-dimensional domain, with realistic constitutive relations (e.g. Brooks-Corey functions) and in case the flow is governed by capillary forces ($p_c \neq 0$). In this benchmark problem the flow occurs in one-dimensional horizontal reservoir, $x \in (0, +\infty)$, initially filled with oil (non-wetting phase), i.e., $S_w(x,0) = S_w^0 = 0,\ \forall x > 0$. The water saturation at the left end of the horizontal column is kept equal to S_{w0}, while the right end is impermeable. Consequently, the total flux vanishes, i.e. $u(x,t) = 0$, at $x \to \infty,\ \forall t \geq 0$. Moreover, there are neither sources ($q_w(x,t) = q_n(x,t) = 0,\ \forall x \geq 0, \forall t \geq 0$) nor gravity terms. Under these assumptions, from system of equations (2a)-(2b), we have that $\forall x \geq 0,\ \forall t \geq 0$

$$\begin{cases} \frac{\partial u}{\partial x} = 0, \\ \Phi \frac{\partial S_w}{\partial t} + \frac{\partial}{\partial x}\left(f_w u + K f_w \lambda_n \frac{dp_c}{dS_w} \frac{\partial S_w}{\partial x} \right) = 0, \\ + \textit{ boundary and initial conditions}, \end{cases}$$

where K is such that $\boldsymbol{K} = K\boldsymbol{I}$. This implies that the total velocity is spatially uniform, but it may vary with time. However, since in Test Case 1, there is no total flux at $x \to \infty,\ \forall t \geq 0$, we get $u(x,t) = 0,\ \forall x \geq 0, \forall t \geq 0$. This represents a bidirectional displacement in which the non-wetting phase (displaced fluid) is draining only at $x = 0$. Under these assumptions, finally, the pressure-saturation formulation provides the following equation for the saturation of the wetting phase S_w, $\forall x \in (0, +\infty),\ t \in (0, +\infty)$

$$\Phi \frac{\partial S_w}{\partial t} + \frac{\partial}{\partial x}\left(K f_w \lambda_n \frac{dp_c}{dS_w} \frac{\partial S_w}{\partial x} \right) = 0. \tag{17}$$

Moreover, we consider the following initial and boundary conditions

$$\begin{aligned} &S_w = S_w^0, \quad x > 0, \quad t = 0, \\ &S_w = S_{w0}, \quad x = 0, \quad t > 0, \\ &S_w = S_w^0, \quad x \to \infty, \quad t > 0, \end{aligned} \tag{18}$$

with $S_{w0} > S_w^0$ constant values. The wetting phase, that is the displacing phase, is pumped inside the domain at $x = 0$ with boundary flux u_{w0}. It can be proved that choosing u_{w0} so that it is inversely proportional to the square root of time, i.e., $u_{w0} = At^{-\frac{1}{2}}$, the governing partial differential equation (17) reduces to a single non-linear second order differential equation known as the McWhorter and Sunada equation [37]. This can be solved quasi-analytically though an iterative integral procedure. The constant A is related to the ability of the porous medium to imbibe fluid at the boundary [36].

7.2 Test Case 2: Unidirectional flow

In Test Case 1 we assume the existence of an impermeable boundary at $x \to \infty$. In Test Case 2, we consider a completely permeable boundary at $x \to \infty$ with no resistance to the flow, so that $u(x,t) = u_{w0} = At^{-\frac{1}{2}},\ \forall x \geq 0,\ \forall t \geq 0$. This represents a unidirectional flow. Given this, the pressure-saturation formulation provides the following more general equation for the saturation of the wetting phase S_w, $\forall x \in (0, +\infty),\ t \in (0, +\infty)$

$$\Phi \frac{\partial S_w}{\partial t} + \frac{\partial}{\partial x}\Big(f_w u + K f_w \lambda_n \frac{dp_c}{dS_w} \frac{\partial S_w}{\partial x} \Big) = 0, \tag{19}$$

It is possible to show that under these conditions, the more the initial value of the saturation of the wetting phase S_{w0} at the inlet $x = 0$ increases, the more the capillary pressure becomes negligible and equation (19) tends to a non-linear first-order hyperbolic equation known as the Buckley-Leverett equation

$$\Phi \frac{\partial S_w}{\partial t} + u \frac{\partial f_w}{\partial x} = 0.$$

8 Numerical results

In this subsection we report and discuss the numerical results obtained by means of our numerical method. In order to evaluate the quality of our numerical solutions, we need to compare them with the quasi-analytical solutions. The solution presented by McWhorter and Sunada is in the form of an iterative integral equation [47]. However, this traditional approach may suffer from convergence issues due to large values of the saturation of the wetting phase at the inlet. As a consequence, we compute the semi-analytical solution relying on the more robust and accurate approach proposed by Bjørnarå and Mathias in [36] that involves the use of pseudospectral Chebyshev differentiation matrices. This allows us to compute the saturation of the wetting phase S_w for a given time as a function of x. In order to compute the pressure of the non-wetting phase p_n, we rely on equation (3). In Test Case 1 the total velocity $u = 0$. Therefore, the expression of the pressure is given by

$$p_n(x) = \int_0^x \frac{\lambda_w}{\lambda} \frac{dp_c}{dS_w} \frac{\partial S_w}{\partial x}\, \mathrm{d}x + p_{n_0}, \tag{20}$$

where p_{n_0} denotes the pressure of the non-wetting phase at $x = 0$. In Test Case 2 the total velocity $u = At^{-\frac{1}{2}}$. Therefore, the expression of the pressure is given by

$$p_n(x) = \int_0^x \Big(\frac{\lambda_w}{\lambda} \frac{dp_c}{dS_w} \frac{\partial S_w}{\partial x} - \frac{At^{-\frac{1}{2}}}{K\lambda} \Big)\, \mathrm{d}x + p_{n_0}. \tag{21}$$

In particular, our aim is to compare our numerical solutions with the ones reported in paper [37]. We point out that since the initial saturation of the wetting phase equals zero, it can happen that in its temporal evolution the numerical solution S_{w_δ} attains negative values in certain points of

the domain very close to the points where S_{w_δ} equals zero. However, this is not acceptable neither from a physical point of view nor from a mathematical point of view. Indeed, physically $S_w \in [0,1]$, and some integrals of the variational formulation contain terms such as the following ones that are not computable for a generic value of μ, if S_{w_δ} attains negative values

$$\lambda_w \frac{dp_c}{dS_w} = -\frac{p_d}{\mu\mu_w(1-S_{wr}-S_{nr})}\bar{S}_w^{\frac{2\mu+1}{\mu}}, \quad \lambda_w = \frac{\bar{S}_w^{\frac{2+3\mu}{\mu}}}{\mu_w}, \quad \lambda = \frac{\bar{S}_w^{\frac{2+3\mu}{\mu}}}{\mu_w} + \frac{\bar{S}_n^2\Big(1-(1-\bar{S}_n)^{\frac{2+\mu}{\mu}}\Big)}{\mu_n}.$$

In order to cope with this problem, we decided to adopt a local correction of S_{w_δ}. This means that we set to zero only the values that are negative on the quadrature nodes that are used to evaluate the parameters in the computation of the integrals, but we do not change the global solution setting to zero the negative values after each Newton iteration. We choose this approach, because a global correction causes a forward shift of the front that becomes quite evident especially in the saturation solution of Test Case 2. Whereas, applying a local correction we can guarantee the computation of the terms appearing in the integrals and, at the same, we do not push forward the position of the front. However, as a major drawback, we are forced to accept negative values of the saturation near the front. Moreover, we have qualitatively observed that this local correction seems no not perturb too much the solution. To verify this we have set $\mu = 1$, so that the previous terms are computable even for negative values of S_{w_δ} and we have compared the solutions obtained with and without the local correction observing a negligible difference.

8.1 nGJV stabilization

In Section 7.2 we have noticed that for McWhorter and Sunada unidirectional flow problem, the more the initial value of the saturation of the wetting phase S_{w0} at the inlet increases, the more the capillary pressure becomes negligible and the equation for the saturation degenerates into a non-linear hyperbolic equation. Consequently, the proposed VEM gives rise to unstable solutions. Therefore, we need to introduce a suitable numerical stabilization technique. In particular, we focus on a non-linear stabilization technique involving a localized non-linear artificial viscosity $\epsilon(S_{w_\delta})$ depending on the solution itself that should mitigate spurious oscillations. The non-linear stabilization term has the form

$$(\epsilon(S_{w_\delta})\Pi^0_{k_s-1}\nabla S_{w_\delta}, \Pi^0_{k_s-1}\nabla v_{S_\delta}).$$

To define $\epsilon(S_{w_\delta})$ we resort to a modified version of the so-called Gradient Jump Viscosity method (GJV). The idea of GJV methods is to scale the artificial diffusion considering the jump of the gradient among the elements of the mesh. In particular, we focus on a formulation that makes use of the nodal jump and mean values, therefore called nodal Gradient Jump Viscosity method (nGJV). Adapting the nGJV method exposed in [38] to our purposes, we define the artificial viscosity term as

$$\epsilon(S_{w_\delta})|_E = const||\tilde{\beta}||_{L^\infty(E)} \max_{\boldsymbol{x}_i \in \mathcal{M}_\delta(E)} \Big(\frac{[\![\Pi^0_{k_s-1}\nabla S_{w_\delta}]\!]_i}{2\{\!\{|\Pi^0_{k_s-1}\nabla S_{w_\delta}|\}\!\}_i}\Big)^q,$$

where *const* and $q > 0$ are suitable selected constants, $\tilde{\beta} = \frac{d\lambda_w}{dS_w}\boldsymbol{K}\Pi^0_{k-1}\nabla p_{n_\delta}$ is an approximation of the velocity vector field of the transport problem, $\mathcal{M}_\delta(E)$ is the set of nodes of the element E, $[\![\Pi^0_{k_s-1}\nabla S_{w_\delta}]\!]_i$ is the jump of $\Pi^0_{k_s-1}\nabla S_{w_\delta}$ on the node $\boldsymbol{x}_i$, $\{\!\{|\Pi^0_{k_s-1}\nabla S_{w_\delta}|\}\!\}$ is the mean value of $|\Pi^0_{k_s-1}\nabla S_{w_\delta}|$ on the node $\boldsymbol{x}_i$. Theoretically, the jump and the mean value of $\Pi^0_{k_s-1}\nabla S_{w_\delta}$ are defined as follows

$$[\![\Pi^0_{k_s-1}\nabla S_{w_\delta}]\!]_i = \max_{\boldsymbol{r}\in\mathbb{S}^d}\lim_{\lambda\to 0}(\Pi^0_{k_s-1}\nabla S_{w_\delta}(\boldsymbol{x}_i+\lambda\boldsymbol{r})\cdot\boldsymbol{r} - \Pi^0_{k_s-1}\nabla S_{w_\delta}(\boldsymbol{x}_i-\lambda\boldsymbol{r})\cdot\boldsymbol{r}),$$

$$\{\!\{\Pi^0_{k_s-1}\nabla S_{w_\delta}\}\!\}_i = \frac{1}{2}\max_{\boldsymbol{r}\in\mathbb{S}^d}\lim_{\lambda\to 0}(\Pi^0_{k_s-1}\nabla S_{w_\delta}(\boldsymbol{x}_i+\lambda\boldsymbol{r})\cdot\boldsymbol{r} + \Pi^0_{k_s-1}\nabla S_{w_\delta}(\boldsymbol{x}_i-\lambda\boldsymbol{r})\cdot\boldsymbol{r}),$$

where $\mathbb{S}^d \subset \mathbb{R}^d$ is the unit sphere. Numerically, we cannot evaluate $\Pi^0_{k_s-1}\nabla S_{w_\delta}$ along all the infinite directions passing through the point $\boldsymbol{x}_i$. Therefore, given a node $\boldsymbol{x}_i$, we consider only the directions going from the barycentre of the elements sharing node $\boldsymbol{x}_i$ to the node $\boldsymbol{x}_i$ itself.

8.2 Test Case 1

We consider our numerical resolution of the McWhorter and Sunada problem for the bidirectional flow on a bi-dimensional domain. In order to validate the approach, we use a setup consisting of artificially selected values for the parameters of the porous medium and of the fluids taken from paper [37]. The domain and the time interval are $\Omega = (0, 0.3) \times (0, 1)$ $[m^2]$ and $\mathcal{I}_T = [0, 1000]$ $[s]$, respectively. The data related to the porous medium and the fluids are reported in Table 2 and the boundary and initial conditions are reported in Table 3. We denote by $\boldsymbol{n}$ the unit normal pointing outward associated with the boundary of the square domain Ω. We underline that since the total normal velocity $\boldsymbol{u} \cdot \boldsymbol{n}$ is constant in space at the right edge of the square domain Ω and the saturation of the wetting phase vanishes after the front, when needed we can decrease the domain along the x-axis without changing the boundary conditions at the right edge of the square domain Ω. Consequently, we do not need to use the same domain limits of paper [37], i.e. $x \in (0, 1)$ $[m]$, in order to compare the solutions.

Porosity	$\Phi = 0.3$ $[-]$
Absolute permeability	$\boldsymbol{K} = 10^{-10} \cdot \mathbf{I}$ $[m^2]$
Residual saturations	$S_{wr} = 0,\ S_{nr} = 0$ $[-]$
Viscosities	$\mu_w = 0.001,\ \mu_n = 0.020$ $[Pa \cdot s]$
Brooks-Corey parameters	$\mu = 2.0$ $[-],\ p_d = 1000$ $[Pa]$

Table 2 Porous medium and fluids data for the bidirectional flow (McWhorter and Sunada)

$y = 0$ and $y = 1$ $[m]$	$\boldsymbol{u} \cdot \boldsymbol{n} = 0$ $[m \cdot s^{-1}],\ \boldsymbol{u}_w \cdot \boldsymbol{n} = 0$ $[m \cdot s^{-1}]$
$x = 0$ $[m]$	$p_n = 2 \cdot 10^5$ $[Pa],\ \ S_w = 0.8$ $[-]$
$x = 0.3$ $[m]$	$\boldsymbol{u} \cdot \boldsymbol{n} = 0$ $[m \cdot s^{-1}],\ S_w = 0$ $[-]$
$x \in \Omega,\ t = 0$ $[s]$	$S_w(x, 0) = 0$ $[-]$

Table 3 Boundary and initial conditions for the bidirectional flow (McWhorter and Sunada)

To show that refining the mesh the numerical solution converges to the actual solution, we compute the L^2-norm of the difference between p_{n_δ} and the semi-analytical solution for the pressure of the non-wetting phase and the L^2-norm of the difference between S_{w_δ} and the semi-analytical solution for the saturation of the wetting phase, for four different refinements. The considered grids are similar to those described in Section 6 and reported in Figure 1. We underline that we do not possess the analytical expressions of the exact solutions. Indeed, we have computed them through the semi-analytical approach and so we only know an approximation of their values at certain points of the domain. In addition, these points are not uniformly distributed because Chebyshev nodes are used in the procedure exposed in [36]. As a consequence, the computation of the L^2-norms of the errors cannot be considered sufficiently accurate for the computation of an exact rate of convergence. Furthermore, since we do not know the actual dependence of the solutions on time, we do not have a priori estimates on the order of convergence and on the expected slopes of the curves reported in Figure 5. Nevertheless, our aim is just to verify that the error decreases when refining the mesh. The estimates of the L^2-norms of the errors for VEM order $k = 1$ at $t = 1000$ $[s]$ and different types of tessellations are reported in Figure 5.

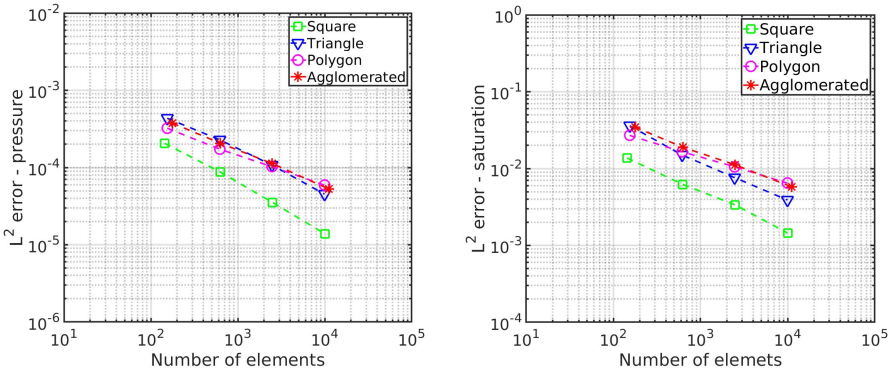

(a) Pressure, $k = 1$, L^2 error **(b)** Saturation, $k = 1$, L^2 error

Figure 5 Estimate of the L^2 error for the pressure p_n and for the saturation S_w at $t = 1000$ $[s]$, using the semi-analytical solutions for VEM order $k = 1$

In Figure 6 we compare qualitatively the graphs of the semi-analytical solution (6a) constructed using the method of paper [36] and the numerical solution (6b) for the saturation of the wetting phase S_w. In particular, we show the numerical solutions obtained at $t = 1000$ $[s]$ using a mesh consisting of 9939 polygonal elements and a VEM spatial discretization of order $k = 1$.

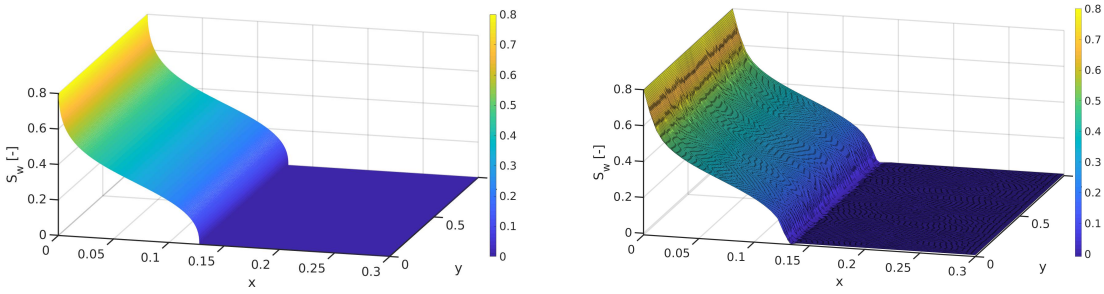

(a) S_w: semi-analytical solution **(b)** S_w: numerical solution

Figure 6 Saturation S_w, McWhorter and Sunada, bidirectional flow: comparison between the semi-analytical solution and the numerical solution for VEM order $k = 1$ at $t = 1000$ $[s]$, on a uniform grid of polygons, $\Omega = (0, 0.3) \times (0, 1)$ $[m^2]$

In Figure 7 we compare qualitatively the graphs of the semi-analytical solution (7a) constructed integrating numerically expression (20) and the numerical solution (7b) for the pressure of the non-wetting phase p_n.

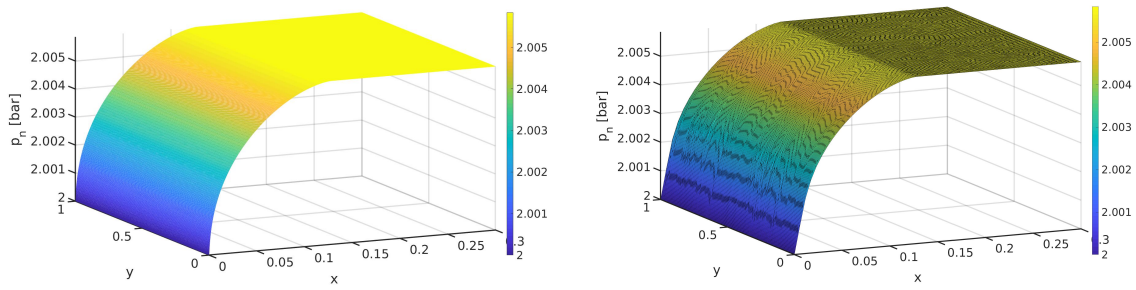

(a) p_n: semi-analytical solution

(b) p_n: numerical solution

Figure 7 Pressure p_n, McWhorter and Sunada, bidirectional flow: comparison between the semi-analytical solution and the numerical solution for VEM order $k = 1$ at $t = 1000$ $[s]$, on a uniform grid of polygons, $\Omega = (0, 0.3) \times (0, 1)$ $[m^2]$

Figures 6 and 7 involve a uniform refinement of the polygonal grid. Indeed, to better capture the behaviour of the solution we have displayed a detail of the solution with $x \in (0, 0.3)$ $[m]$. The full solutions for the same domain of paper [37], $\Omega \in (0, 1) \times (0, 1)$ $[m^2]$, are reported in Figures 8 and 9 at time $t = 1000$ $[s]$. These solutions are obtained on a refined triangle mesh in the region around $x = 0.2$.

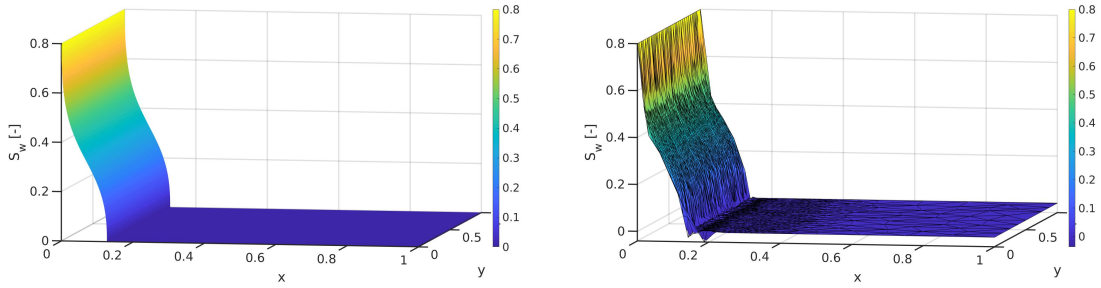

(a) S_w: semi-analytical solution

(b) S_w: numerical solution

Figure 8 Saturation S_w, McWhorter and Sunada, bidirectional flow: comparison between the semi-analytical solution and the numerical solution for VEM order $k = 1$ at $t = 1000$ $[s]$ on a locally refined triangle grid , $\Omega = (0, 1) \times (0, 1)$ $[m^2]$

As discussed at the beginning of Section 8, since we only perform a local correction of the saturation in the evaluation of the parameters and not a global one in the solution, the numerical saturation S_{w_δ} displays negative values close to the points in the region of transition from high gradients to flat zero values. We can see this phenomenon in Figure 8b.

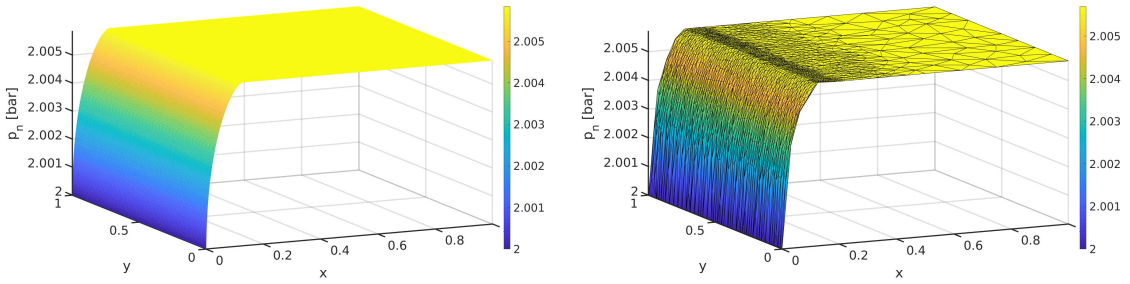

(a) p_n: semi-analytical solution

(b) p_n: numerical solution

Figure 9 Pressure p_n, McWhorter and Sunada, bidirectional flow: comparison between the semi-analytical solution and the numerical solution for VEM order $k = 1$ at $t = 1000$ $[s]$ on a locally refined triangle grid, $\Omega = (0,1) \times (0,1)$ $[m^2]$

8.3 Test Case 2

We consider our numerical resolution of the McWhorter and Sunada problem for the unidirectional flow on a bi-dimensional domain. In order to validate the approach, we use the same parameters of the porous medium and of the fluids used in Test Case 1 and reported in Table 2. Moreover, the domain and the time interval of the problem are $\Omega = (0,1) \times (0,1)$ $[m^2]$ and $\mathcal{I}_T = [0, 1000]$ $[s]$, respectively. The boundary and initial conditions are reported in Table 4. The main difference with respect to Taste Case 1 concerns the boundary condition for the pressure of the non-wetting phase at the right boundary of the domain $(1, y)$, $\forall y \in (0,1)$. Indeed, in Test Case 1, the total velocity vanished at the outlet, whereas in Test Case 2, the total velocity achieves its maximum, i.e., $At^{-\frac{1}{2}}$, at the outlet.

$y = 0$ and $y = 1$ $[m]$	$\boldsymbol{u} \cdot \boldsymbol{n} = 0$ $[m \cdot s^{-1}]$, $\boldsymbol{u}_w \cdot \boldsymbol{n} = 0$ $[m \cdot s^{-1}]$
$x = 0$ $[m]$	$p_n = 2 \cdot 10^5$ $[Pa]$, $S_w = S_{w0}$ $[-]$
$x = 1$ $[m]$	$\boldsymbol{u} \cdot \boldsymbol{n} = A \cdot t^{-\frac{1}{2}}$ $[m \cdot s^{-1}]$, $S_w = 0$ $[-]$
$x \in \Omega$, $t = 0$ $[s]$	$S_w(x, 0) = 0$ $[-]$

Table 4 Boundary and initial conditions for the unidirectional flow (McWhorter and Sunada)

In the numerical simulations, we consider increasing values of S_{w0} approaching the limiting case $S_{w0} = 1$, i.e., we analyse the behaviour of the numerical saturation of the wetting phase $S_{w\delta}$ as the original convective-diffusive parabolic problem becomes gradually more and more convective dominated until it reaches the limiting case of a pure hyperbolic problem. The values of S_{w0} considered are reported in Table 5 together with the values of the related coefficients A. The values of A have been computed using the method proposed in paper [36] and adopting the Brooks-Corey model for the capillary pressure-saturation function and the relative permeabilities-saturation functions.

S_{w0} $[-]$	A $[m \cdot s^{-\frac{1}{2}}]$
0.6	4.8790e-04
0.8	2.0271e-03
0.9	5.4769e-03

Table 5 Values of S_{w0} and A for the unidirectional flow

Given the boundary conditions reported in Table 4, we can notice that the Neumann boundary

condition for the pressure equation at $x = 1$ $[m]$ and for time $t = 0$ $[s]$ goes to infinity. To avoid such a problem we start the numerical computation from $t = 0.1$ $[s]$ and we set $S_w(x, 0.1) = S_{w0.1}$ as initial condition for our numerical simulation. Here, $S_{w0.1}$ corresponding to the values S_{w0} of Table 5 are approximated using the semi-analytical procedure presented in paper [36]. We show the numerical solutions obtained at $t = 1000$ $[s]$ using a mesh consisting of 9911 polygonal elements and a VEM spatial discretization of order $k = 1$. The results of the numerical simulations for increasing values of S_{w0} are reported in Figure 10 for the saturation of the wetting phase. In this figure we compare qualitatively the graphs of the semi-analytical solutions (10a and 10c) and the numerical solutions (10b and 10d) for the saturation of the wetting phase. We report only the extreme cases, i.e., $S_{w0} = 0.6$ and $S_{w0} = 0.9$. The numerical solution for the case $S_{w0} = 0.8$ reproduces quite accurately the semi-analytical solution similarly to the case $S_{w0} = 0.6$.

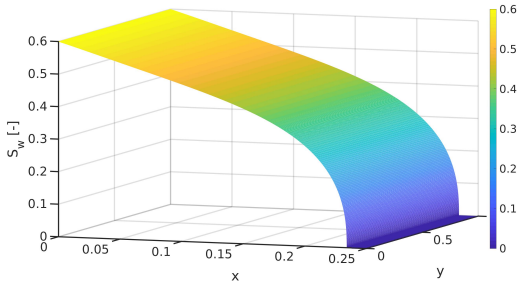

(a) S_w: semi-analytical solution, $S_{w0} = 0.6$

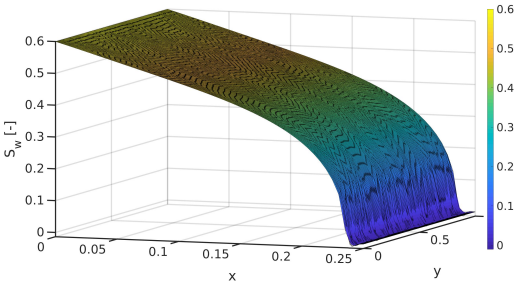

(b) S_w: numerical solution, $S_{w0} = 0.6,\ \mathcal{N}_\delta = 9911,\ \Delta t = 1.25\ s$

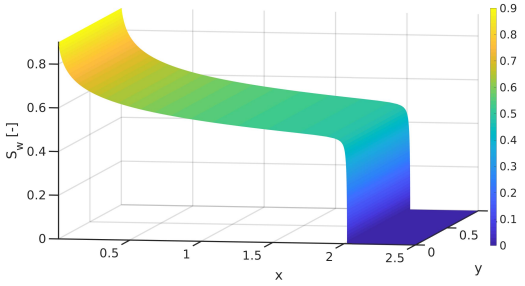

(c) S_w: semi-analytical solution, $S_{w0} = 0.9$

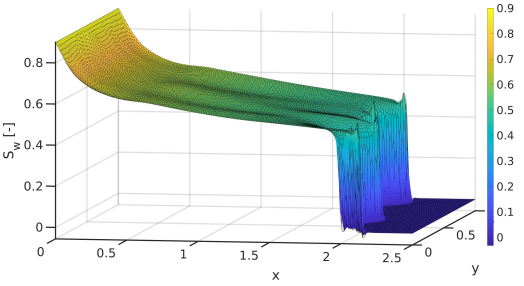

(d) S_w: numerical solution, $S_{w0} = 0.9,\ \mathcal{N}_\delta = 9911,\ \Delta t = 0.125\ s$

Figure 10 Saturation S_w, McWhorter and Sunada, unidirectional flow: increasing values of S_{w0}, polygonal meshes, VEM order $k = 1$, at $t = 1000$ $[s]$

Figures 10b and 10d show qualitatively that the more the initial saturation S_{w0} increases, that is, the more the parabolic case approaches the hyperbolic case, the more the numerical solution for the saturation of the wetting phase get worse. In particular, in Figure 10d we can see that the numerical saturation is characterized by several oscillations that become very strong in the region around the front of the solution. We have further observed that relevant benefits can be obtained on a sufficiently refined mesh by adding the nGJV stabilization described in Section 8.1. Indeed, if we add the non-linear stabilization with $const = 0.0005$ and $q = 1$, we obtain Figure 11a, instead of Figure 10d. We can see that the numerical solution arising from the stabilized problem is characterized by a reduction of the oscillations and a more regular approximation of the front.

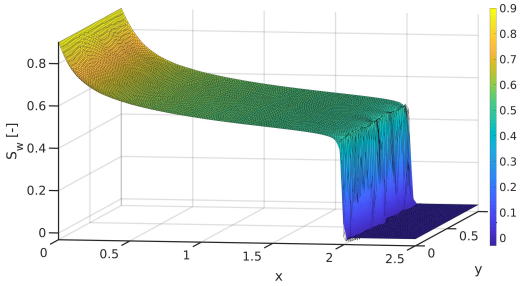

(a) S_w: VEM + nGJV numerical solution, $S_{w0} = 0.9,\ \mathcal{N}_\delta = 9911,\ \Delta t = 0.125\ s$.

Figure 11 Saturation S_w, McWhorter and Sunada, unidirectional flow: polygonal mesh, VEM order $k = 1$, $t = 1000\ [s]$

In Figure 12 we compare qualitatively the graphs of the semi-analytical solution (12a and 12c) and the numerical solution (12b and 12d) for the pressure of the non-wetting phase.

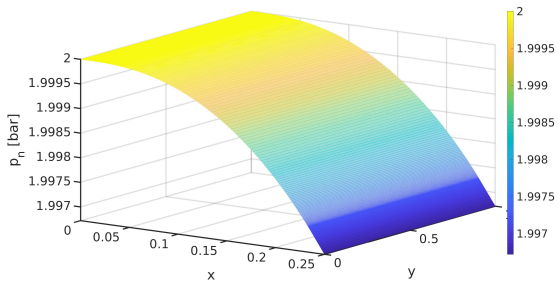

(a) p_n: semi-analytical solution, $S_{w0} = 0.6$

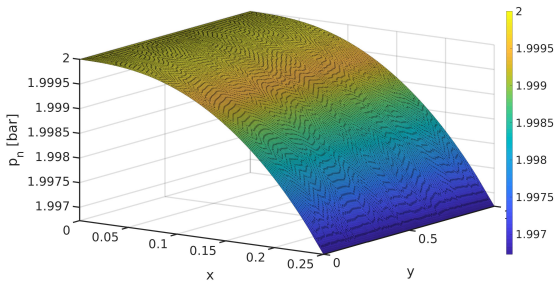

(b) p_n: numerical solution, $S_{w0} = 0.6,\ \mathcal{N}_\delta = 9911,\ \Delta t = 1.25\ s$

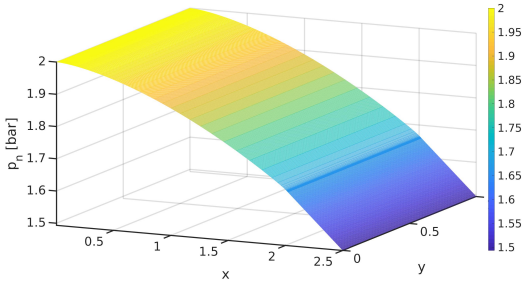

(c) p_n: semi-analytical solution, $S_{w0} = 0.9$

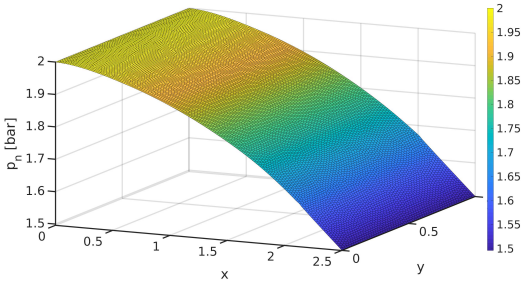

(d) S_w: numerical solution, $S_{w0} = 0.9,\ \mathcal{N}_\delta = 9911,\ \Delta t = 0.125\ s$

Figure 12 Pressure p_n, McWhorter and Sunada, unidirectional flow: increasing values of S_{w0}, polygonal meshes, VEM order $k = 1$, $t = 1000\ [s]$

In Figure 13, we report the number of Newton iterations that are needed in Test Case 2 in order to satisfy the convergence criteria introduced in Section 5 ($tol_1 = 10^{-16}$, $tol_2 = 10^{-5}$). In particular, in Figure 13a, we show the number of Newton iterations for the case $S_{w0} = 0.6$, a polygonal mesh having $\mathcal{N}_{\delta_1} = 9911$ elements and a time step $\Delta t = 1.25\ [s]$. Whereas, in Figure 13b, we show the number of Newton iterations for the case $S_{w0} = 0.9$, a polygonal mesh having $\mathcal{N}_{\delta_1} = 9911$ elements and a time step $\Delta t = 0.125\ [s]$. In this figure we also provide a comparison between the number of Newton iterations that are needed with and without the nGJV stabilization. We can see that it does not change significantly. In both Figure 13a and Figure 13b, we can see that at the beginning the number of Newton iterations is close to 25, but then, for most of the

time instants it remains below 5.

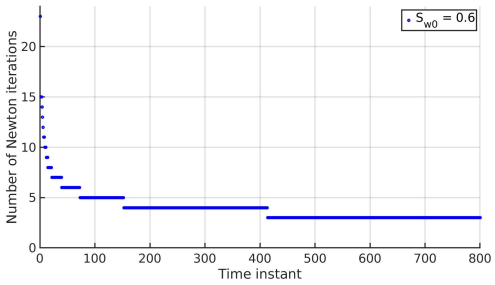

(a) $S_{w0} = 0.6$, polygonal mesh $\mathcal{N}_\delta = 9911$, $\Delta t = 1.25\ s$

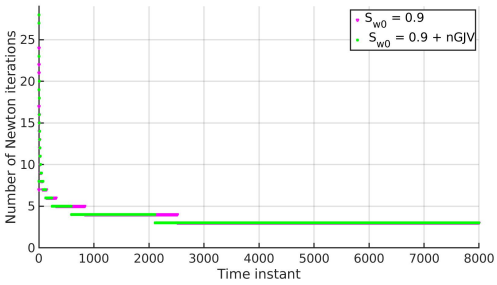

(b) $S_{w0} = 0.9$, polygonal mesh $\mathcal{N}_\delta = 9911$, $\Delta t = 0.125\ s$

Figure 13 Newton iterations for Test Case 2

9 Conclusions

In this work, we have proposed and analysed a time and space discretization of the two-phase flow equations of immiscible fluids in porous media through an iterative IMplicit-Pressure-Implicit-Saturation method coupled with a primal C^0-conforming VEM. The numerical results have confirmed the effectiveness of the approach in dealing with both the coupled non-linear nature of the involved equations and non-standard polygonal meshes. We have highlighted the robustness of the VEM with respect to the geometry of the grids, empathizing the potentialities of this method in tackling problems characterized by complex geometries. Moreover, we have qualitatively observed that when the parabolic equation for the saturation eventually degenerates into a hyperbolic equation, the application of nGJV stabilization to the VEM seems to provide relevant benefits in smoothing or eliminating the oscillatory behaviours of the numerical solution on a sufficiently refined mesh. This work is intended as a contribution to the framework of numerical techniques for applications in porous media.

Acknowledgements

We acknowledge that the present research was partially supported by a MIUR Grant-Dipartimenti di Eccellenza 2018-2022 n. E11G18000350001, by the MIUR PRIN Project 201744KLJL_004 and by INdAM GNCS. Computational resources were partially provided by HPC@PoliTO and SmartData@PoliTO.

References

[1] L. B. da Veiga, K. Lipnikov, G. Manzini, The mimetic finite difference method for elliptic problems, Vol. 11, Springer, 2014.

[2] L. Beirão da Veiga, F. Brezzi, A. Cangiani, G. Manzini, L. D. Marini, A. Russo, Basic principles of virtual element methods, Mathematical Models and Methods in Applied Sciences 23 (01) (2013) 199–214. doi:https://doi.org/10.1142/S0218202512500492.

[3] B. A. de Dios, K. Lipnikov, G. Manzini, The nonconforming virtual element method, ESAIM: Mathematical Modelling and Numerical Analysis 50 (3) (2016) 879–904. doi:https://doi.org/10.1051/m2an/2015090.

[4] B. Ahmad, A. Alsaedi, F. Brezzi, L. D. Marini, A. Russo, Equivalent projectors for virtual element methods, Computers & Mathematics with Applications 66 (3) (2013) 376–391. doi:https://doi.org/10.1016/j.camwa.2013.05.015.

[5] L. Beirão da Veiga, F. Brezzi, L. Marini, A. Russo, Virtual element method for general second-order elliptic problems on polygonal meshes, Mathematical Models and Methods in Applied Sciences 26 (04) (2016) 729–750. doi:https://doi.org/10.1142/S0218202516500160.

[6] S. Berrone, A. Borio, G. Manzini, SUPG stabilization for the nonconforming virtual element method for advection–diffusion–reaction equations, Computer Methods in Applied Mechanics and Engineering 340 (2018) 500–529. doi:https://doi.org/10.1016/j.cma.2018.05.027.

[7] A. Cangiani, G. Manzini, O. J. Sutton, Conforming and nonconforming virtual element methods for elliptic problems, IMA Journal of Numerical Analysis 37 (3) (2017) 1317–1354. doi:https://doi.org/10.1093/imanum/drw036.

[8] G. Vacca, L. Beirão da Veiga, Virtual element methods for parabolic problems on polygonal meshes, Numerical Methods for Partial Differential Equations 31 (6) (2015) 2110–2134. doi:https://doi.org/10.1002/num.21982.

[9] G. Vacca, Virtual element methods for hyperbolic problems on polygonal meshes, Computers & Mathematics with Applications 74 (5) (2017) 882–898. doi:https://doi.org/10.1016/j.camwa.2016.04.029.

[10] F. Brezzi, R. S. Falk, L. D. Marini, Basic principles of mixed virtual element methods, ESAIM: Mathematical Modelling and Numerical Analysis 48 (4) (2014) 1227–1240. doi:https://doi.org/10.1051/m2an/2013138.

[11] L. B. da Veiga, F. Brezzi, L. D. Marini, A. Russo, Mixed virtual element methods for general second order elliptic problems on polygonal meshes, ESAIM: Mathematical Modelling and Numerical Analysis 50 (3) (2016) 727–747. doi:https://doi.org/10.1051/m2an/2015067.

[12] L. B. Da Veiga, F. Brezzi, L. Marini, A. Russo, Serendipity nodal VEM spaces, Computers & Fluids 141 (2016) 2–12. doi:https://doi.org/10.1016/j.compfluid.2016.02.015.

[13] L. Beirão da Veiga, F. Brezzi, L. D. Marini, A. Russo, The hitchhiker's guide to the virtual element method, Mathematical models and methods in applied sciences 24 (08) (2014) 1541–1573. doi:https://doi.org/10.1142/S021820251440003X.

[14] E. Cáceres, G. N. Gatica, A mixed virtual element method for the pseudostress–velocity formulation of the Stokes problem, IMA Journal of Numerical Analysis 37 (1) (2017) 296–331. doi:https://doi.org/10.1093/imanum/drw002.

[15] L. B. da Veiga, C. Lovadina, G. Vacca, Divergence free virtual elements for the stokes problem on polygonal meshes, ESAIM: Mathematical Modelling and Numerical Analysis 51 (2) (2017) 509–535. doi:https://doi.org/10.1051/m2an/2016032.

[16] E. Artioli, S. De Miranda, C. Lovadina, L. Patruno, A stress/displacement virtual element method for plane elasticity problems, Computer Methods in Applied Mechanics and Engineering 325 (2017) 155–174. doi:https://doi.org/10.1016/j.cma.2017.06.036.

[17] F. Brezzi, L. D. Marini, Virtual element methods for plate bending problems, Computer Methods in Applied Mechanics and Engineering 253 (2013) 455–462. doi:https://doi.org/10.1016/j.cma.2012.09.012.

[18] L. B. Da Veiga, F. Brezzi, L. D. Marini, Virtual elements for linear elasticity problems, SIAM Journal on Numerical Analysis 51 (2) (2013) 794–812. doi:https://doi.org/10.1137/120874746.

[19] M. F. Benedetto, S. Berrone, S. Scialò, A globally conforming method for solving flow in discrete fracture networks using the virtual element method, Finite Elements in Analysis and Design 109 (2016) 23–36. doi:https://doi.org/10.1016/j.finel.2015.10.003.

[20] S. Berrone, A. Borio, Orthogonal polynomials in badly shaped polygonal elements for the virtual element method, Finite Elements in Analysis and Design 129 (2017) 14–31. doi:https://doi.org/10.1016/j.finel.2017.01.006.

[21] S. Berrone, A. Borio, A residual a posteriori error estimate for the virtual element method, Mathematical Models and Methods in Applied Sciences 27 (08) (2017) 1423–1458. doi:https://doi.org/10.1142/S0218202517500233.

[22] S. Berrone, A. Borio, A. D'Auria, Refinement strategies for polygonal meshes applied to adaptive VEM discretization, Finite Elements in Analysis and Design 186 (2019) 103502. doi:https://doi.org/10.1016/j.finel.2020.103502.

[23] L. B. Da Veiga, F. Brezzi, F. Dassi, L. Marini, A. Russo, Virtual element approximation of 2d magnetostatic problems, Computer Methods in Applied Mechanics and Engineering 327 (2017) 173–195. doi:https://doi.org/10.1016/j.cma.2017.08.013.

[24] P. F. Antonietti, L. B. Da Veiga, S. Scacchi, M. Verani, A C^1 virtual element method for the Cahn–Hilliard equation with polygonal meshes, SIAM Journal on Numerical Analysis 54 (1) (2016) 34–56. doi:https://doi.org/10.1137/15M1008117.

[25] D. Adak, E. Natarajan, S. Kumar, Convergence analysis of virtual element methods for semi-linear parabolic problems on polygonal meshes, Numerical Methods for Partial Differential Equations 35 (1) (2019) 222–245. doi:https://doi.org/10.1002/num.22298.

[26] L. B. da Veiga, C. Lovadina, G. Vacca, Virtual Elements for the Navier–Stokes Problem on Polygonal Meshes, SIAM Journal on Numerical Analysis 56 (3) (2018) 1210–1242. doi:https://doi.org/10.1137/17M1132811.

[27] E. Artioli, L. Veiva, C. Lovadina, E. Sacco, Arbitrary order 2D virtual elements for polygonal meshes: Part II, inelastic problem, Computational Mechanics 60. doi:https://doi.org/10.1007/s00466-017-1429-9.

[28] A. Cangiani, P. Chatzipantelidis, G. Diwan, E. H. Georgoulis, Virtual element method for quasilinear elliptic problems, IMA Journal of Numerical Analysis 40 (4) (2020) 2450–2472. doi:https://doi.org/10.1093/imanum/drz035.

[29] L. Beirão da Veiga, A. Pichler, G. Vacca, A virtual element method for the miscible displacement of incompressible fluids in porous media, Computer Methods in Applied Mechanics and Engineering 375 (2021) 113649. doi:https://doi.org/10.1016/j.cma.2020.113649.

[30] Z. Chen, G. Huan, Y. Ma, Computational methods for multiphase flows in porous media, SIAM, 2006.

[31] D. W. Peaceman, Fundamentals of numerical reservoir simulation, Elsevier, 2000.

[32] R. Helmig, et al., Multiphase flow and transport processes in the subsurface: a contribution to the modeling of hydrosystems., Springer-Verlag, 1997.

[33] B. Amaziane, S. Antontsev, L. Pankratov, A. Piatnitski, Homogenization of immiscible compressible two-phase flow in porous media: application to gas migration in a nuclear waste repository, Multiscale Modeling & Simulation 8 (5) (2010) 2023–2047. doi:https://doi.org/10.1137/100790215.

[34] G. Chavent, J. Jaffré, Mathematical models and finite elements for reservoir simulation: single phase, multiphase and multicomponent flows through porous media, Elsevier, 1986.

[35] A. Kvashchuk, F. A. Radu, A Fully-Implicit, Iterative Scheme for the Simulation of Two-Phase Flow in Porous Media, in: European Conference on Numerical Mathematics and Advanced Applications, Springer, 2017, pp. 625–633. doi:https://doi.org/10.1007/978-3-319-96415-7_57.

[36] T. I. Bjørnarå, S. A. Mathias, A pseudospectral approach to the McWhorter and Sunada equation for two-phase flow in porous media with capillary pressure, Computational Geosciences 17 (6) (2013) 889–897. doi:http://dx.doi.org/10.1007/s10596-013-9360-4.

[37] R. Fučík, J. Mikyška, M. Beneš, T. H. Illangasekare, An improved semi-analytical solution for verification of numerical models of two-phase flow in porous media, Zone Journal 6 (1) (2007) 93–104. doi:https://doi.org/10.2136/vzj2006.0024.

[38] A. Hierro Fabregat, Monotonicity preserving shock capturing techniques for finite elements, Ph.D. thesis, Universitat Politècnica DE Catalunya (2016).

[39] A. Fumagalli, Numerical modelling of flows in fractured porous media by the XFEM method, Ph.D. thesis, Italy (2012).

[40] R. H. Brooks, A. T. Corey, Hydraulic properties of porous media, Colorado State University, Hydrology and Water Resources Program, 1964.

[41] P. Bastian, Numerical Computation of Multiphase Flow in Porous Media, Ph.D. thesis, Christian-Albrechts-Universität Kiel (1999).

[42] J. E. Aarnes, T. Gimse, K.-A. Lie, An introduction to the numerics of flow in porous media using Matlab, in: Geometric modelling, numerical simulation, and optimization, Springer, 2007, pp. 265–306. doi:https://doi.org/10.1007/978-3-540-68783-2_9.

[43] J. Kou, S. Sun, On iterative IMPES formulation for two phase flow with capillarity in heterogeneous porous media, International Journal of Numerical Analysis and Modeling. Series B 1 (1) (2010) 20–40.

[44] J. Lions, E. Magenes, Non-homogeneous boundary value problems and applications: vol. I and II Springer-Verlag, Berlin, 1972.

[45] J. R. Shewchuk, Triangle: Engineering a 2D quality mesh generator and Delaunay triangulator, in: Workshop on Applied Computational Geometry, Springer, 1996, pp. 203–222. doi:https://doi.org/10.1007/BFb0014497.

[46] C. Talischi, G. H. Paulino, A. Pereira, I. F. Menezes, PolyMesher: a general-purpose mesh generator for polygonal elements written in Matlab, Structural and Multidisciplinary Optimization 45 (3) (2012) 309–328. doi:https://doi.org/10.1007/s00158-011-0706-z.

[47] D. B. McWhorter, D. K. Sunada, Exact integral solutions for two-phase flow, Water Resources Research 26 (3) (1990) 399–413. doi:https://doi.org/10.1029/WR026i003p00399.